

# Tension and constraints on modified gravity parametrizations of $G_{\text{eff}}(z)$ from growth rate and Planck data

Savvas Nesseris,<sup>1,\*</sup> George Pantazis,<sup>2,†</sup> and Leandros Perivolaropoulos<sup>3,‡</sup><sup>1</sup>*Instituto de Física Teórica UAM-CSIC, Universidad Autónoma de Madrid, Cantoblanco, 28049 Madrid, Spain*<sup>2</sup>*Department of Physics, University of Ioannina, GR-45110 Ioannina, Greece*<sup>3</sup>*Department of Physics, University of Patras, GR-26500 Patras, Greece*

(Received 3 April 2017; published 31 July 2017)

We construct an updated and extended compilation of growth-rate data based on recent redshift-space distortion measurements. The data set consists of 34 data points and includes corrections for model dependence. In order to minimize overlap and maximize the independence of the data points, we also construct a subsample of this compilation (a “gold” growth data set) which consists of 18 data points. We test the consistency of this data set with the best-fit Planck15/ $\Lambda$ CDM parameters in the context of General Relativity using the evolution equation for the growth factor  $\delta(a)$  with a  $w$ CDM background. We find tension at the  $\sim 3\sigma$  level between the best-fit parameters  $w$  (the dark energy equation of state),  $\Omega_{0m}$  (the matter density parameter), and  $\sigma_8$  (the matter power spectrum normalization on scales  $8h^{-1}$  Mpc) and the corresponding Planck15/ $\Lambda$ CDM parameters ( $w = -1$ ,  $\Omega_{0m} = 0.315$ , and  $\sigma_8 = 0.831$ ). We show that the tension disappears if we allow for evolution of the effective Newton constant, parametrized as  $G_{\text{eff}}(a)/G_{\text{N}} = 1 + g_a(1-a)^n - g_a(1-a)^{2n}$  with  $n \geq 2$  where  $g_a$  and  $n$  are parameters of the model,  $a$  is the scale factor, and  $z = 1/a - 1$  is the redshift. This parametrization satisfies three important criteria: a) positive energy of the graviton ( $G_{\text{eff}} > 0$ ), b) consistency with big bang nucleosynthesis constraints ( $G_{\text{eff}}(a \ll 1)/G_{\text{N}} = 1$ ), and c) consistency with Solar System tests ( $G_{\text{eff}}(a = 1)/G_{\text{N}} = 1$  and  $G'_{\text{eff}}(a = 1)/G_{\text{N}} = 0$ ). We show that the best-fit form of  $G_{\text{eff}}(z)$  obtained from the growth data corresponds to weakening gravity at recent redshifts (decreasing function of  $z$ ), and we demonstrate that this behavior is not consistent with any scalar-tensor Lagrangian with a real scalar field. Finally, we use MGCAMB to find the best-fit  $G_{\text{eff}}(z)$  obtained from the Planck cosmic microwave background power spectrum on large angular scales and show that it is a mildly increasing function of  $z$ , in  $3\sigma$  tension with the corresponding decreasing best-fit  $G_{\text{eff}}(z)$  obtained from the growth data.

DOI: [10.1103/PhysRevD.96.023542](https://doi.org/10.1103/PhysRevD.96.023542)

## I. INTRODUCTION

Despite the vast improvement in quality and quantity of the cosmological observations during the past 18 years, the simplest cosmological model predicting an accelerating expansion of the Universe, known as the  $\Lambda$ CDM [1], has remained viable and consistent with observations [2–4]. Crucial assumptions of this model are the validity of General Relativity (GR) on cosmological scales, flatness homogeneity, isotropy, and the invariance of dark energy in both space and time (cosmological constant). The parameters of this model have been pinned down to extraordinary accuracy by the Planck [5] mission. These parameter values define the concordance Planck15/ $\Lambda$ CDM model and are shown in Table I. This model is consistent with a wide range of independent cosmological observations

testing mainly the large scale cosmological background  $H(z)$ . Such observations include earlier analyses of cosmic microwave background (CMB) fluctuations [6], large scale velocity flows [7], baryon acoustic oscillations [8,9], Type Ia supernovae [10], early growth rate of perturbations data [11–14], gamma ray burst data [15–17], strong and weak lensing data [18],  $H(z)$  (Hubble parameter) data [19], HII galaxy data [20], and cluster gas mass fraction data [21,22].

Despite the consistency of Planck15/ $\Lambda$ CDM with large cosmological scales background data, it has become evident recently that a mild tension appears to exist between Planck15/ $\Lambda$ CDM and some independent observations in intermediate cosmological scales ( $z \leq 0.6$ ), [23]. Such tensions include estimates of the Hubble parameter [24–30] in the context of, estimates of the amplitude of the power spectrum on the scale of  $8h^{-1}$  Mpc ( $\sigma_8$ ) [1], and estimates of the matter density parameter  $\Omega_{0m}$  [31].

In addition, there are theoretical arguments based on naturalness that may hint toward physics beyond the concordance  $\Lambda$ CDM model [2–4].

\*savvas.nesseris@csic.es

†gpantaz@cc.uoi.gr

‡On leave from Department of Physics, University of Ioannina, GR-45110 Ioannina, Greece. leandros@uoi.gr

TABLE I. Planck15/ $\Lambda$ CDM parameters with 68% limits. Based on TT, TE, EE + lowP and a flat  $\Lambda$ CDM model (middle column) or a  $w$ CDM model (right column); see Table 4 of Ref. [5] and the Planck chains archive.<sup>a</sup>

Parameter	Value ( $\Lambda$ CDM)	Value ( $w$ CDM)
$\Omega_b h^2$	$0.02225 \pm 0.00016$	$0.02229 \pm 0.00016$
$\Omega_c h^2$	$0.1198 \pm 0.0015$	$0.1196 \pm 0.0015$
$n_s$	$0.9645 \pm 0.0049$	$0.9649 \pm 0.0048$
$H_0$	$67.27 \pm 0.66$	$> 81.3$
$\Omega_m$	$0.3156 \pm 0.0091$	$0.203_{-0.065}^{+0.022}$
$w$	$-1$	$-1.55_{-0.38}^{+0.19}$
$\sigma_8$	$0.831 \pm 0.013$	$0.983_{-0.055}^{+0.100}$

<sup>a</sup>A probability distribution function (pdf) describing the data contained in the Planck archive can be found here: [https://wiki.cosmos.esa.int/planckpla2015/index.php/Cosmological\\_Parameters](https://wiki.cosmos.esa.int/planckpla2015/index.php/Cosmological_Parameters).

The data that are in some tension with Planck15/ $\Lambda$ CDM appear to indicate consistently that there is a lack of gravitational power in structures on intermediate-small cosmological scales. This lack of power may be expressed through different cosmological parameters in a degenerate manner. For example, it may be expressed as a lower value of  $\Omega_{0m}$  at redshifts less than about 0.6 or as a smaller value of  $\sigma_8$  or as a dark energy equation of state that becomes smaller than  $-1$  at low redshifts.

The situation is reminiscent of the corresponding situation in the early 1990s before the confirmation of  $\Lambda$ CDM by Supernovae type Ia (SnIa) data [32,33] when the Einstein-de Sitter flat “standard CDM model” was seen to be in mild tension with a range of cosmological data on large cosmological data including the COBE discovery of large scale CMB fluctuations which were larger than expected in the CDM model. It was first realized by Efstathiou in 1990 that there is more power on large scales than predicted by CDM [34] and that a flat universe with a cosmological constant could ease the large scale tension. This analysis was confirmed by other subsequent studies [35–39]. Despite the evidence that the CDM model lacked the required power on large scales to match observations, it remained the “standard model” until 1998 when the accelerating expansion was confirmed at several  $\sigma$  using type Ia supernovae [32,33].

The parameter that is most commonly used to describe the lack of power of Planck15/ $\Lambda$ CDM on small scales is the variance of the linear matter perturbations on  $8h^{-1}$  Mpc,  $\sigma_8$ . This parameter can be obtained from a weak lensing correlation function obtained by the CFHTLenS Collaboration [40], from the galaxy cluster count [41], and from redshift-space distortion (RSD) data [42,43]. These data sets indicate that there is lower growth power than the one inferred in the context of Planck15/ $\Lambda$ CDM and GR, at about  $2\sigma$  level [44–46]. This tension, if not due to systematics, could be reconciled by a mechanism that reduces the rate of

clustering between recombination and today. Three such possible mechanisms are as follows:

- (i) A hot dark matter component induced, e.g., by a sterile neutrino [47].
- (ii) Dark matter clusters differently at small and large scales, a possibility explored in Ref. [48].
- (iii) Modifications of GR [49] which attenuate the growth rate of perturbations.

In the present study, we focus on the third mechanism. If a modification of GR is responsible for the observed cosmological accelerating expansion, it would also lead to a modified growth rate of cosmological density perturbations compared to the one predicted in GR. This growth rate has been measured in several surveys in redshifts ranging from  $z = 0.02$  up to  $z = 1.4$  and is defined as

$$f(a) = \frac{d\delta(a)}{d \ln a}, \quad (1.1)$$

where  $\delta(a) \equiv \frac{\delta\rho}{\rho}$  denotes the cosmological overdensity and  $a(t)$  is the scale factor.

Most growth-rate measurements are obtained using peculiar velocities obtained from RSD measurements [50] identified in galaxy redshift surveys. In general, such surveys can provide measurements of the perturbations in terms of the galaxy density  $\delta_g$ , which are related to matter perturbations through the bias parameter  $b$  as  $\delta_g = b\delta_m$ . Thus, early growth-rate measurements provided values of the growth rate  $f$  divided by the bias factor  $b$  leading to the parameter  $\beta_b^f$ .

This measured parameter is sensitive to the value of the bias  $b$  which can vary in the range  $b \in [1, 3]$ . This uncertainty factor makes it difficult to combine values of  $\beta$  from different regions and different surveys leading to unreliable data sets of  $\beta(z_i)$ .

A more reliable combination is the product  $f(z)\sigma_8(z) \equiv f\sigma_8(z)$ , as it is independent of the bias and may be obtained using either weak lensing or RSD. Thus, in the present study, we only consider surveys that have reported the growth rate in the robust form  $f(z)\sigma_8(z)$ . These surveys along with the corresponding data points are shown in Table II where the data are shown in chronological order, along with the assumed fiducial cosmology and other notes, e.g., their covariance matrix and so on.

Some of these points are in fact highly correlated with other points since they were produced by analyses of the same sample of galaxies. Also, it is clear from Table II that there has been a dramatic increase and improvement of the growth-rate data during the past five years. This is mainly due to the SDSS, BOSS, WiggleZ, and Vipers surveys that have dramatically increased the number of growth-rate data and their constraining power. The quality and quantity of the growth-rate data are expected to improve dramatically in the coming years with the Euclid [51] and LSST [52] surveys.

TABLE II. A collection of recent  $f\sigma_8(z)$  measurements from different surveys, ordered chronologically. In the columns, we show the name and year of the survey that made the measurement, the redshift and value of  $f\sigma_8(z)$ , and the corresponding reference and fiducial cosmology. These data points are not independent and should not be used altogether at the same time. For a robust compilation, see Table III.

Index	Data set	$z$	$f\sigma_8(z)$	Refs.	Year	Notes
1	SDSS-LRG	0.35	$0.440 \pm 0.050$	[58]	2006	$(\Omega_m, \Omega_K) = (0.25, 0)$
2	VVDS	0.77	$0.490 \pm 0.18$	[58]	2008	$(\Omega_m, \Omega_K) = (0.25, 0)$
3	2dFGRS	0.17	$0.510 \pm 0.060$	[58]	2009	$(\Omega_m, \Omega_K) = (0.3, 0)$
4	2MASS	0.02	$0.314 \pm 0.048$	[59,60]	2010	$(\Omega_m, \Omega_K) = (0.266, 0)$
5	SnIa + IRAS	0.02	$0.398 \pm 0.065$	[61,60]	2011	$(\Omega_m, \Omega_K) = (0.3, 0)$
6	SDSS-LRG-200	0.25	$0.3512 \pm 0.0583$	[62]	2011	$(\Omega_m, \Omega_K) = (0.25, 0)$
7	SDSS-LRG-200	0.37	$0.4602 \pm 0.0378$	[62]	2011	
8	SDSS-LRG-60	0.25	$0.3665 \pm 0.0601$	[62]	2011	$(\Omega_m, \Omega_K) = (0.25, 0)$
9	SDSS-LRG-60	0.37	$0.4031 \pm 0.0586$	[62]	2011	
10	WiggleZ	0.44	$0.413 \pm 0.080$	[63]	2012	$(\Omega_m, h) = (0.27, 0.71)$
11	WiggleZ	0.60	$0.390 \pm 0.063$	[63]	2012	$C_{ij} \rightarrow \text{Eq. (2.8)}$
12	WiggleZ	0.73	$0.437 \pm 0.072$	[63]	2012	
13	SDSS-BOSS	0.30	$0.407 \pm 0.055$	[64]	2012	$(\Omega_m, \Omega_K) = (0.25, 0)$
14	SDSS-BOSS	0.40	$0.419 \pm 0.041$	[64]	2012	
15	SDSS-BOSS	0.50	$0.427 \pm 0.043$	[64]	2012	
16	SDSS-BOSS	0.60	$0.433 \pm 0.067$	[64]	2012	
17	SDSS-DR7-LRG	0.35	$0.429 \pm 0.089$	[65]	2012	$(\Omega_m, \Omega_K) = (0.25, 0)$
18	6dFGRS	0.067	$0.423 \pm 0.055$	[66]	2012	$(\Omega_m, \Omega_K) = (0.27, 0)$
19	GAMA	0.18	$0.360 \pm 0.090$	[67]	2013	$(\Omega_m, \Omega_K) = (0.27, 0)$
20	GAMA	0.38	$0.440 \pm 0.060$	[67]	2013	
21	BOSS-LOWZ	0.32	$0.384 \pm 0.095$	[68]	2013	$(\Omega_m, \Omega_K) = (0.274, 0)$
22	SDSS-CMASS	0.59	$0.488 \pm 0.060$	[69]	2013	$(\Omega_m, h, \sigma_8) = (0.307115, 0.6777, 0.8288)$
23	Vipers	0.80	$0.470 \pm 0.080$	[70]	2013	$(\Omega_m, \Omega_K) = (0.25, 0)$
24	SDSS-MGS	0.15	$0.490 \pm 0.145$	[71]	2014	$(\Omega_m, h, \sigma_8) = (0.31, 0.67, 0.83)$
25	SDSS-veloc	0.10	$0.370 \pm 0.130$	[72]	2015	$(\Omega_m, \Omega_K) = (0.3, 0)$
26	FastSound	1.40	$0.482 \pm 0.116$	[73]	2015	$(\Omega_m, \Omega_K) = (0.270, 0)$
27	6dFGS + SnIa	0.02	$0.428 \pm 0.0465$	[74]	2016	$(\Omega_m, h, \sigma_8) = (0.3, 0.683, 0.8)$
28	Vipers PDR-2	0.60	$0.550 \pm 0.120$	[75]	2016	$(\Omega_m, \Omega_b) = (0.3, 0.045)$
29	Vipers PDR-2	0.86	$0.400 \pm 0.110$	[75]	2016	
30	BOSS DR12	0.38	$0.497 \pm 0.045$	[76]	2016	$(\Omega_m, \Omega_K) = (0.31, 0)$
31	BOSS DR12	0.51	$0.458 \pm 0.038$	[76]	2016	
32	BOSS DR12	0.61	$0.436 \pm 0.034$	[76]	2016	
33	Vipers v7	0.76	$0.440 \pm 0.040$	[77]	2016	$(\Omega_m, \sigma_8) = (0.308, 0.8149)$
34	Vipers v7	1.05	$0.280 \pm 0.080$	[77]	2016	

Despite the dramatic improvement of the quality and quantity of the growth-rate data, their combination into a single uniform and self-consistent data set remains a challenge. There are two basic reasons for this:

- (i) Model dependence: Since surveys do not measure distances to galaxies directly, they have to assume a specific cosmological model in order to infer distances. All growth-rate data points shown in Table II assume a flat  $\Lambda$ CDM cosmological background albeit with different  $\Omega_{0m}$  and/or  $\sigma_8$ . The actual values of these parameters used for each data point are shown in Table II. This model dependence requires a correction before the data are included in a single uniform data set.
- (ii) Double-counting: Some of the data points shown in Table II correspond to the same sample of galaxies

analyzed by different groups/methods, and the inclusion of all these points without proper corrections would lead to double-counting and artificial decrease of the error regions.

In the present analysis, we address the above issues and construct a new large, uniform, and reliable growth-rate data set which consists of independent data points that are corrected for model dependence by rescaling growth-rate measurements by proper ratios of  $H(z)D_A(z)$  where  $D_A(z)$  is the angular diameter distance. We use this data set to investigate the tension level with a Planck15/ $\Lambda$ CDM background model under the assumption of validity of GR.

The tension we find can be eliminated by either changing the background Hubble parameter  $H(z)$  or by allowing modifications of GR through a scale independent effective Newton constant  $G_{\text{eff}}(z)$ . We follow that latter route, and

assuming that the Planck15/ $\Lambda$ CDM background is correct, we find the best-fit form of  $G_{\text{eff}}(z)$  using the Planck15/ $\Lambda$ CDM  $H(z)$  and our growth-rate data set. The derivation of the best-fit effective Newton's constant along with the Planck15/ $\Lambda$ CDM  $H(z)$  allows the reconstruction of the underlying fundamental model Lagrangian density in the context of specific classes of models.

A general and generic such class of models is scalar-tensor theories where the action in the Jordan frame is determined by the scalar field potential  $U(\phi)$  and the nonminimal coupling  $F(\phi)$  in the form

$$\mathcal{S} = \int d^4x \sqrt{-g} \left[ \frac{1}{2} F(\phi) R - \frac{1}{2} Z(\phi) g^{\mu\nu} \partial_\mu \phi \partial_\nu \phi - U(\phi) \right] + S_m, \quad (1.2)$$

where  $R$  is the Ricci scalar. We have set  $8\pi G_N \equiv 1$  for simplicity (and therefore  $F_0 = 1$  at the present time), and  $S_m$  is the matter action of some arbitrary matter fields, i.e., does not involve the scalar field  $\phi$ . Even though the scalar field is fully described by the set of  $F(\phi)$ ,  $Z(\phi)$ , and  $U(\phi)$ , a convenient reduction to two parameters can be applied (e.g., Refs. [53–55]) by a rescaling of the scalar field. For example, we may have the Brans-Dicke reduction where  $F(\phi) = \phi$ ,  $Z(\phi) = \omega(\phi)/\phi$ , or alternatively we can obtain  $Z(\phi) = 1$  with arbitrary  $F(\phi)$  as done in the present analysis. We note that all of the above are applied in the Jordan frame where the model is studied. In addition,  $F(\phi) > 0$  is required so that gravitons have positive energy and  $dF/d\phi < 4 \times 10^{-4}$  according to Solar System tests (see Refs. [54,56]). As discussed in Sec. IV, the effective

Newton constant  $G_{\text{eff}}(z)$  is approximately inversely proportional to the nonminimal coupling  $F(\phi(z))$  and is observable through the growth of cosmological perturbations.

It is thus possible to use the best-fit form of  $G_{\text{eff}}(z)$  along with the Planck15/ $\Lambda$ CDM  $H(z)$  to reconstruct the underlying scalar-tensor theory potential  $U(\phi)$  that would produce the observed functional forms of  $G_{\text{eff}}(z)$  and  $H(z)$ . This scalar-tensor theory is defined by the functional forms of the scalar field potential  $U(\phi)$  and nonminimal coupling  $F(\phi)$  that are reconstructed uniquely using the method of Refs [53,54,57]. However, as also noted in Ref. [54], this task is not always possible as the reconstructed kinetic term of the scalar field in many cases becomes negative at some redshift range  $z$ , i.e.,  $\phi'(z)^2 < 0$ , and as a result, the field itself becomes imaginary. In what follows, we derive the properties of functions  $F(z)$  that lead to positive kinetic terms for a real scalar field when used in a reconstruction. These properties come from the fact that  $F(z)$  satisfies a differential inequality, and we can deduce them by using the Chaplygin theorem on differential inequalities.

The structure of this paper is the following. In the next section, we introduce the new robust and extended growth data set (Table III) and use it to investigate the tension level between growth data and Planck15/ $\Lambda$ CDM in the context of GR. In Sec. III, we allow for extensions of GR and introduce  $G_{\text{eff}}(z)$  parametrizations consistent with Solar System tests and nucleosynthesis. We then find the best-fit form of  $G_{\text{eff}}(z)$  for each parametrization and investigate the effect of the evolving Newton's constant on the tension between growth data and Planck15/ $\Lambda$ CDM. In Sec. IV, we use the best-fit forms of  $G_{\text{eff}}(z)$  to implement the

TABLE III. A compilation of robust and independent  $f\sigma_8(z)$  measurements from different surveys, based on Table II. In the columns, we show in ascending order with respect to redshift the name and year of the survey that made the measurement, the redshift and value of  $f\sigma_8(z)$ , and the corresponding reference and fiducial cosmology. These data points are used in our analysis in the next sections.

Index	Data set	$z$	$f\sigma_8(z)$	Refs.	Year	Notes
1	6dFGS + SnIa	0.02	$0.428 \pm 0.0465$	[74]	2016	$(\Omega_m, h, \sigma_8) = (0.3, 0.683, 0.8)$
2	SnIa + IRAS	0.02	$0.398 \pm 0.065$	[61,60]	2011	$(\Omega_m, \Omega_K) = (0.3, 0)$
3	2MASS	0.02	$0.314 \pm 0.048$	[59,60]	2010	$(\Omega_m, \Omega_K) = (0.266, 0)$
4	SDSS-veloc	0.10	$0.370 \pm 0.130$	[72]	2015	$(\Omega_m, \Omega_K) = (0.3, 0)$
5	SDSS-MGS	0.15	$0.490 \pm 0.145$	[71]	2014	$(\Omega_m, h, \sigma_8) = (0.31, 0.67, 0.83)$
6	2dFGRS	0.17	$0.510 \pm 0.060$	[58]	2009	$(\Omega_m, \Omega_K) = (0.3, 0)$
7	GAMA	0.18	$0.360 \pm 0.090$	[67]	2013	$(\Omega_m, \Omega_K) = (0.27, 0)$
8	GAMA	0.38	$0.440 \pm 0.060$	[67]	2013	
9	SDSS-LRG-200	0.25	$0.3512 \pm 0.0583$	[62]	2011	$(\Omega_m, \Omega_K) = (0.25, 0)$
10	SDSS-LRG-200	0.37	$0.4602 \pm 0.0378$	[62]	2011	
11	BOSS-LOWZ	0.32	$0.384 \pm 0.095$	[68]	2013	$(\Omega_m, \Omega_K) = (0.274, 0)$
12	SDSS-CMASS	0.59	$0.488 \pm 0.060$	[69]	2013	$(\Omega_m, h, \sigma_8) = (0.307115, 0.6777, 0.8288)$
13	WiggleZ	0.44	$0.413 \pm 0.080$	[63]	2012	$(\Omega_m, h) = (0.27, 0.71)$
14	WiggleZ	0.60	$0.390 \pm 0.063$	[63]	2012	$C_{ij} \rightarrow \text{Eq. (2.8)}$
15	WiggleZ	0.73	$0.437 \pm 0.072$	[63]	2012	
16	Vipers PDR-2	0.60	$0.550 \pm 0.120$	[75]	2016	$(\Omega_m, \Omega_b) = (0.3, 0.045)$
17	Vipers PDR-2	0.86	$0.400 \pm 0.110$	[75]	2016	
18	FastSound	1.40	$0.482 \pm 0.116$	[73]	2015	$(\Omega_m, \Omega_K) = (0.270, 0)$

reconstruction method for the derivation of the underlying scalar-tensor potential. We find that for the particular form of the best-fit  $G_{\text{eff}}(z)$  no consistent reconstruction of a realistic scalar-tensor model can be implemented due to the fact that the kinetic term of the scalar field becomes negative, i.e.,  $\phi'(z)^2 < 0$ . Then, by using the Chaplygin theorem on differential inequalities, we derive the required properties of the observed  $G_{\text{eff}}(z)$  in the context of a  $\Lambda$ CDM background so that a well-defined scalar-tensor theory can be reconstructed. In Sec. V, we determine the effects of the  $G_{\text{eff}}(z)$  parametrization on the low- $\ell$  multipoles of the CMB, while in Sec. VI, we conclude, summarize, and discuss future extensions of the present work.

## II. EXTENDED CALIBRATED GROWTH RSD DATA SET: TENSION WITH Planck15/ $\Lambda$ CDM

### A. Theoretical background

In order to discriminate between GR and modified gravity theories, we need an extra observational probe which can track the dynamical properties of gravity. One such probe is the growth function of the linear matter density contrast  $\delta \equiv \frac{\delta\rho_m}{\rho_m}$ , where  $\rho_m$  represents the background matter density and  $\delta\rho_m$  represents its first-order perturbation.

It can be shown that in many classes of modified gravity theories the growth factor  $\delta(a)$  satisfies the following equation [78–81],

$$\delta''(a) + \left(\frac{3}{a} + \frac{H'(a)}{H(a)}\right)\delta'(a) - \frac{3\Omega_m G_{\text{eff}}(a, k)/G_N}{2a^5 H(a)^2/H_0^2}\delta(a) = 0, \quad (2.1)$$

where primes denote differentiation with respect to the scale factor,  $H(a) \equiv \frac{\dot{a}}{a}$  is the Hubble parameter, and  $G_{\text{eff}}(a, k)$  is the effective Newton constant which is constant and equal to  $G_N$  in GR. In modified gravity theories,  $G_{\text{eff}}$  depends on both the scale factor  $a$  (or equivalently the redshift  $z$ ) and the scale  $k$ . However,  $G_{\text{eff}}$  is independent of the scale  $k$  for scales smaller than the horizon ( $k \gg aH$ ) [82]. Thus, on subhorizon scales, we may ignore the dependence on the scale  $k$  for both  $\delta$  and  $G_{\text{eff}}$ .

For the growing mode, we assume the initial conditions  $\delta(a \ll 1) = a$  and  $\delta'(a \ll 1) = 1$ , where in practice we will choose a small enough value of the scale factor so that we are well within the matter domination era, e.g.,  $a_{\text{ini}} \sim 10^{-3}$ . Note that this equation is only valid on subhorizon scales, i.e.,  $k^2 \gg a^2 H^2$ , where  $k$  is the wave number of the modes of the perturbations in Fourier space. The effects of modified gravity theories enter Eq. (2.1) via both  $H(a)$  and  $G_{\text{eff}}(a, k)$ . This is due to the fact that the growth of the large scale structure is a result of the motion of matter and therefore is sensitive to both the expansion of the Universe and the evolution of Newton's ‘‘constant’’.

In the case of GR, the exact solution of Eq. (2.1) for a flat model with a constant dark energy equation of state  $w$  is given for the growing mode by [83,84]

$$\delta(a) = a \cdot {}_2F_1\left(-\frac{1}{3w}, \frac{1}{2} - \frac{1}{2w}; 1 - \frac{5}{6w}; a^{-3w}(1 - \Omega_m^{-1})\right), \quad (2.2)$$

where  ${}_2F_1(a, b; c; z)$  is a hypergeometric function defined by the series

$${}_2F_1(a, b; c; z) \equiv \frac{\Gamma(c)}{\Gamma(a)\Gamma(b)} \sum_{n=0}^{\infty} \frac{\Gamma(a+n)\Gamma(b+n)}{\Gamma(c+n)n!} z^n \quad (2.3)$$

on the disk  $|z| < 1$  and by analytic continuation elsewhere (see Ref. [85] for more details). In general, it is impossible to find analytical solutions to Eq. (2.1) for a generic modified gravity model, so numerical methods for solving it have to be used.

As discussed in the Introduction, a robust measurable quantity in redshift surveys is not the growth factor  $\delta(a)$ . Instead, it is the combination

$$f\sigma_8(a) \equiv f(a) \cdot \sigma(a) = \frac{\sigma_8}{\delta(1)} a\delta'(a), \quad (2.4)$$

where  $f(a) = \frac{d \ln \delta}{d \ln a}$  is the growth rate and  $\sigma(a) = \sigma_8 \frac{\delta(a)}{\delta(1)}$  is the redshift-dependent rms fluctuations of the linear density field within spheres of radius  $R = 8h^{-1}$  Mpc, while the parameter  $\sigma_8$  is its value today. This combination is used in what follows to derive constraints for theoretical model parameters.

### B. RSD measurements

Redshift-space distortions are very important probes of large scale structure providing measurements of  $f\sigma_8(a)$ . This can be achieved by measuring the ratio of the monopole and the quadrupole multipoles of the redshift-space power spectrum which depends on  $\beta = f/b$ , where  $f$  is the growth rate and  $b$  is the bias, in a specific way defined by linear theory [58,86,87]. The combination of  $f\sigma_8(a)$  is independent of bias as all bias dependence in this combination cancels out thus, it has been shown that this combination is a good discriminator of DE (Dark energy) models [58].

In Table II, we present a collection of recent  $f\sigma_8(z)$  measurements from different surveys, ordered chronologically. In the columns, we show the name and year of the survey that made the measurement, the redshift, the value of  $f\sigma_8(z)$ , and the corresponding reference and fiducial cosmology. The information in some of these data points

overlaps significantly with other data points in the same table. Some of them are updates on previous measurements either with enhancements in the volume of the survey, during its scheduled run, or with different methodologies by various groups. Therefore, the collection of these data points should not be used in its entirety.

We thus construct the ‘‘Gold-2017’’ compilation of robust and independent  $f\sigma_8(z)$  measurements from different surveys, shown in Table III. In the columns of Table III, we show the name and year of the survey that made the measurement, the redshift, and value of  $f\sigma_8(z)$ , and the corresponding reference and fiducial cosmology. These data points are used in our analysis in the next sections. These points are a subset of those from Table II and were chosen so that only the latest version or more robust version of a measurement is included from every corresponding survey.

In both Tables II and III, the data have a dependence on the fiducial model used by the collaborations to convert redshifts to distances, an important step in the derivations of the data. This can be corrected by either taking into account how the correlation function  $\xi(r)$  transforms by changing the cosmology, an approach followed by Ref. [88], or by simply rescaling the growth-rate measurements by the ratios of  $H(z)D_A(z)$  of the cosmology used to that of the fiducial one as in Ref. [89]. As noted in Ref. [89], the correction itself is quite small, so we follow the latter method for simplicity.

Specifically, we implement the correction as follows. First, we define the ratio of the product of the Hubble parameter  $H(z)$  and the angular diameter distance  $d_A(z)$  for the model at hand to that of the fiducial cosmology, i.e.,

$$\text{ratio}(z) = \frac{H(z)d_A(z)}{H^{fid}(z)d_A^{fid}(z)}, \quad (2.5)$$

where the values of the fiducial cosmology, namely  $\Omega_{0m}$ , are given in Table III. Note that the combination  $H(z)d_A(z)$  does not depend on  $H_0$ , so it could be equivalently written in terms of the dimensionless Hubble parameter  $E(z) = H(z)/H_0$  and angular diameter distance  $D_A(z) = \frac{H_0}{c}d_A(z)$ .

Having done this, we can now define the  $\chi^2$  as usual for correlated data. We can define a vector  $V^i(z_i, p^j)$ , where  $z_i$  is the redshift of the  $i$ th point and  $p^j$  is the  $j$ th component of a vector containing the cosmological parameters ( $\Omega_{0m}, w, \sigma_8, \dots$ ) that we want to determine from the data. This vector contains the differences of the data and the theoretical model, after we implement our correction. Specifically, it is given by

$$V^i(z_i, p^j) = f\sigma_{8,i} - \text{ratio}(z_i)f\sigma_8(z_i, p^j), \quad (2.6)$$

where  $f\sigma_{8,i}$  is the value of the  $i$ th data point, with  $i = 1, \dots, N$ , where  $N$  is the total number of points, while  $f\sigma_8(z_i, p^j)$  is the theoretical prediction, both at redshift  $z_i$ .

Then, the  $\chi^2$  can be written as

$$\chi_{\text{growth}}^2 = V^i C_{ij}^{-1} V^j, \quad (2.7)$$

where  $C_{ij}^{-1}$  is the inverse covariance matrix of the data and for compactness we only used the superscripts  $i$  and  $j$  for the data vectors. For an approximation, we will assume that most of the data are not correlated, with the exception of the ones from WiggleZ, where the covariance matrix is given by [63]

$$C_{ij}^{\text{WiggleZ}} = 10^{-3} \begin{pmatrix} 6.400 & 2.570 & 0.000 \\ 2.570 & 3.969 & 2.540 \\ 0.000 & 2.540 & 5.184 \end{pmatrix}. \quad (2.8)$$

Therefore, the total covariance matrix will be the identity  $N \times N$  matrix, but with the addition of a  $3 \times 3$  matrix at the position of the WiggleZ data; i.e., schematically, we could write it as

$$C_{ij}^{\text{growth, total}} = \begin{pmatrix} \sigma_1^2 & 0 & 0 & \dots \\ 0 & C_{ij}^{\text{WiggleZ}} & 0 & \dots \\ 0 & 0 & \dots & \sigma_N^2 \end{pmatrix}. \quad (2.9)$$

An alternative approach would be that of Ref. [88] where the authors approximated the total covariance matrix of all the measurements as the fraction of overlap volume between the surveys to the total volume of the two surveys combined. However, this approach obviously cannot take into account any possible negative correlations between the data as the effect of the correlations can be due to more than the overlapping survey volumes. Thus, this approach can lead to a potentially biased covariance matrix. This issue will be resolved in the near future when upcoming surveys like Euclid and LSST will provide consistent growth-rate measurements in both the low and high redshift regimes.

Using the corrected  $\chi^2$  and our Gold-2017 compilation given by Table III, we now proceed to extract the best-fit cosmological parameters and discuss the results. First, we assume GR with a constant  $w$  model and a flat Universe. Then, the Hubble parameter is given by

$$\begin{aligned} E(a)^2 &\equiv H(a)^2/H_0^2 \\ &= \Omega_{0m}a^{-3} + (1 - \Omega_{0m})a^{-3(1+w)}, \end{aligned} \quad (2.10)$$

where we have ignored the radiation as at late times it has a negligible impact. This case is rather simple, so in order to speed up the code, it is convenient to use the analytical expression for the growing mode of the growth factor given by Eq. (2.2) and the analytical expression for the luminosity distance, which follows after a quick calculation using the definition, given by

$$\frac{H_0}{c}d_L(a) = \frac{2}{a\sqrt{\Omega_{0m}}} {}_2F_1\left(\frac{1}{2}, -\frac{1}{6w}; 1 - \frac{1}{6w}; 1 - \frac{1}{\Omega_m(a)}\right) - \frac{2}{\sqrt{a}\sqrt{\Omega_{0m}}} {}_2F_1\left(\frac{1}{2}, -\frac{1}{6w}; 1 - \frac{1}{6w}; 1 - \frac{1}{\Omega_m(a)}\right), \quad (2.11)$$

where  $\Omega_m(a) = \frac{\Omega_{0m}a^{-3}}{E(a)^2}$ , and then the angular diameter distance is given by  $d_A(z) = \frac{d_L(z)}{(1+z)^2}$  as usual. In the more complicated cases discussed in the next sections, e.g., modified gravity models, we will perform the corresponding calculations numerically.

After fitting the data, we obtain the 68.3%, 95.4%, and 99.7% confidence contours in the  $(w, \sigma_8, \Omega_{0m})$  parameter space, shown in Fig. 1. As it can be seen, the current growth-rate data are at a  $\sim 3\sigma$  tension with the Planck15/ $\Lambda$ CDM best-fit cosmology, indicated with the red dot. For completeness, we also overlap the corresponding Planck15/ $w$ CDM contours even though our goal here is to identify the tension level with Planck15/ $\Lambda$ CDM. We will attempt to alleviate this tension in the next section, by considering modified gravity models, as the extra degrees of freedom provided by the theories may allow a Newton constant of the form  $G_{\text{eff}}(a, k)$  to account for the tension.

Remarkably, we find that, compared to previous studies, e.g., Ref. [90] or even the Planck 2015 data release [5], all of which use outdated growth data, with our new Gold-2017 compilation, we identify a  $3\sigma$  tension. Given the Planck15/ $\Lambda$ CDM background and the fact that we have corrected for the diverse fiducial cosmologies used, this tension could potentially be explained either by assuming that the growth rates  $f\sigma_8$  suffer from a yet unaccounted for systematic or by new physics perhaps affecting either the background  $H(z)$  or inducing an evolution of Newton's constant due to modifications of GR.

In this paper, we will focus on the latter possibility and explore the various possibilities afforded by the rich phenomenology of modified gravity. As mentioned above, in these theories, Newton's constant can be time and scale dependent, i.e.,  $G_{\text{eff}}(a, k)$ , thus affecting the evolution of the growth factor via the last term in Eq. (2.1). We discuss these models in the what follows.

### III. RELEASING THE TENSION USING MODIFIED GRAVITY

In this section, we discuss physically motivated parametrizations of Newton's constant  $G_{\text{eff}}(a, k)$ , paying special attention to scale-independent parametrizations motivated by modified gravity theories on subhorizon scales. We first consider one of the minimal extensions of GR, the well-known  $f(R)$  theories, where it maybe shown that under the subhorizon/quasistatic approximation [79]

$$G_{\text{eff}}/G_N = \frac{1}{F} \frac{1 + 4\frac{k^2}{a^2}m}{1 + 3\frac{k^2}{a^2}m} \quad (3.1)$$

$$m \equiv \frac{F_{,R}}{F} \quad (3.2)$$

$$F \equiv f_{,R} = \frac{\partial f}{\partial R}, \quad (3.3)$$

which reduces to GR only when  $f(R) = R - 2\Lambda$ , i.e., the  $\Lambda$ CDM model, while a more accurate approximation was found in Ref. [91].

One of the simplest extensions of GR and the  $\Lambda$ CDM model with this formalism is the popular  $f(R)$  model of Hu and Sawicki [92]. However, the original form of this model is unnecessarily complicated and has several degenerate parameters, so here we prefer the implementation of the

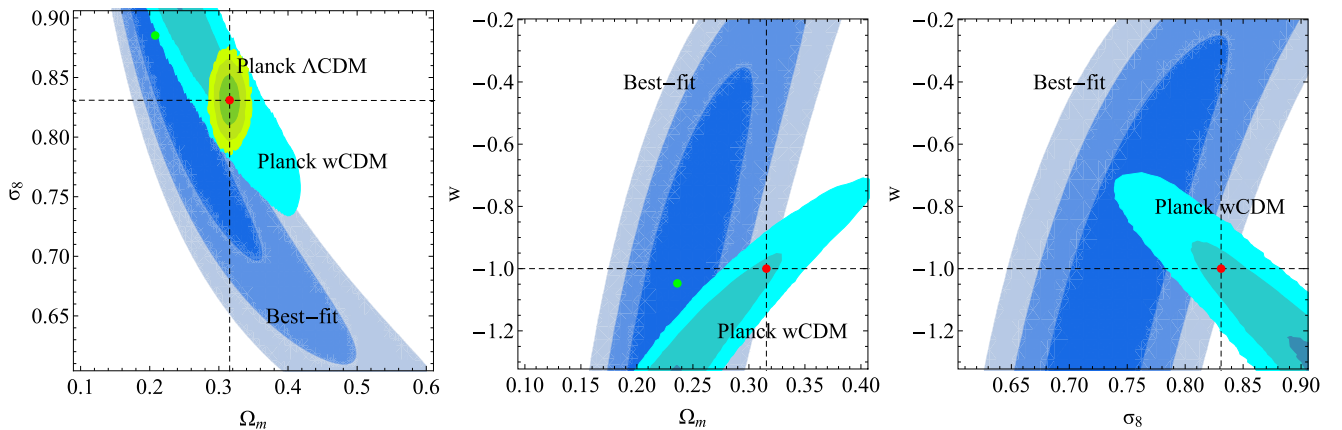


FIG. 1. The 68.3%, 95.4%, and 99.7% confidence contours in the  $(w, \sigma_8, \Omega_{0m})$  parameter space. The red point corresponds to the Planck15/ $\Lambda$ CDM best-fit cosmology, the blue contour corresponds to the best-fit of our data to the  $\Lambda$ CDM model (left) and  $w$ CDM model (middle and right panel), while the light blue and light green contours correspond to the Planck15  $w$ CDM and  $\Lambda$ CDM contours, respectively. As we can see, there is a  $3\sigma$  tension between the Planck15/ $\Lambda$ CDM values and the growth-rate data best fit.

$b$  parameter as in Ref. [93]. This has several useful advantages: first, the deviation of this model from  $\Lambda$ CDM is more transparent, and, second, by performing a Taylor expansion around  $b = 0$ , we can obtain analytical approximations for  $H(z)$  which are accurate to better than 0.1% for  $b \lesssim 1$  and better than  $10^{-5}\%$  for  $b \lesssim 0.1$ . The Lagrangian for the Hu and Sawicki model, as written equivalently in Ref. [93], is

$$f(R) = R - \frac{2\Lambda}{1 + \left(\frac{b\Lambda}{R}\right)^n}, \quad (3.4)$$

where  $n$  is a constant of the model, usually chosen as  $n = 1$  without loss of generality as it only adjusts the steepness of the deviation from the  $\Lambda$ CDM model.

As mentioned, we can also obtain a very accurate Taylor expansion of the solution to the equations of motion around  $b = 0$ , i.e., the  $\Lambda$ CDM model, as

$$H^2(a) = H_\Lambda^2(a) + \sum_{i=1}^M b^i \delta H_i^2(a), \quad (3.5)$$

where

$$\frac{H_\Lambda^2(a)}{H_0^2} = \Omega_{0m} a^{-3} + \Omega_{r0} a^{-4} + (1 - \Omega_{0m} - \Omega_{r0}) \quad (3.6)$$

and  $M$  is the number of terms we keep before truncating the series. However, we have found that keeping only the two first nonzero terms is more than enough to have better than 0.1% accuracy with the numerical solution. The functions  $\delta H_i^2(a)$  are just algebraic expressions and can be easily determined from the equations of motion (see Ref. [93]). Finally, we also follow Ref. [93] and set  $k = 0.1h \text{ Mpc}^{-1} \simeq 300H_0$ , which is necessary as now the Newton constant depends on the scale  $k$  as well.

One can generalize the above model to an action that includes a scalar field with arbitrary kinetic term non-minimally coupled to gravity.<sup>1</sup> Such a model has the following action [79],

$$S = \int d^4x \sqrt{-g} \left( \frac{1}{2} f(R, \phi, X) + \mathcal{L}_m \right), \quad (3.7)$$

where  $X = -g^{\mu\nu} \partial_\mu \phi \partial_\nu \phi$  is the kinetic term of the scalar field. In this case, Newton's constant is given by [79]

<sup>1</sup>Of course, one can also consider other types of theories like models with Galileons or with torsion of the type  $f(T)$ , non-minimal couplings, and so on that have a similar effect. For this paper, we limit ourselves to  $f(R)$  and scalar-tensor theories in order to keep the problem tractable.

$$G_{\text{eff}}(a, k)/G_N = \frac{1}{F} \frac{f_{,X} + 4 \left( f_{,X} \frac{k^2 F_{,R}}{a^2 F} + \frac{F_{,\phi}^2}{F} \right)}{f_{,X} + 3 \left( f_{,X} \frac{k^2 F_{,R}}{a^2 F} + \frac{F_{,\phi}^2}{F} \right)}, \quad (3.8)$$

where  $F = F(R, \phi, X) = \partial_R f(R, \phi, X)$  and  $F_{,\phi} = \partial_\phi F(R, \phi, X)$ . This class of theories encompasses both the  $f(R)$  models and the so called scalar-tensor (ScT) ones, given by the Lagrangian,

$$\mathcal{L}^{\text{ScT}} = \frac{F(\phi)}{2} R + X - U(\phi), \quad (3.9)$$

and in this case, Newton's constant reduces to

$$G_{\text{eff}}(a, k)/G_N = \frac{1}{F(\phi)} \frac{F(\phi) + 2F_{,\phi}^2}{F(\phi) + \frac{3}{2}F_{,\phi}^2}. \quad (3.10)$$

It may be shown that on subhorizon scales both (3.8) and (3.10) are well approximated by scale-independent functions. Thus, in what follows, we ignore the scale dependence of  $G_{\text{eff}}$ .

The effective Newton constant  $G_{\text{eff}}$  can be related to the Friedmann-Robertson-Walker (FRW) metric perturbations and in particular to the Newtonian potentials  $\Phi$  and  $\Psi$  as in Ref. [94], i.e.,

$$ds^2 = a^2 [-(1 + 2\Psi) d\tau^2 + (1 - 2\Phi) d\vec{x}^2], \quad (3.11)$$

$$\nabla^2 \Psi = 4\pi G_N \rho \delta \times G_M, \quad (3.12)$$

$$\nabla^2 (\Phi + \Psi) = 8\pi G_N \rho \delta \times G_L, \quad (3.13)$$

where  $\delta$  is the growth factor and  $G_L$  and  $G_M$  are dimensionless parameters, which are equal to 1 in GR, but otherwise can be parametrized as functions of the scale factor in a variety of ways [94]. In this case,  $G_M = G_{\text{eff}}/G_N$  alters the growth of matter, while  $G_L$  alters the lensing of light via the lensing potential  $\Phi + \Psi$ . Deviations from GR are also described through the gravitational slip defined as

$$\gamma_{\text{slip}} = \frac{\Phi}{\Psi} \quad (3.14)$$

and through the anisotropic stress, that is inherent to most modified gravity theories and is defined as

$$\eta = \frac{\Psi - \Phi}{\Phi}. \quad (3.15)$$

Clearly, the gravitational slip and the anisotropic stress are related via  $\eta = \frac{1}{\gamma_{\text{slip}}} - 1$ , and in GR, we have that  $\gamma_{\text{slip}} = 1$  and  $\eta = 0$ . In Ref. [79], it was shown that in scalar-tensor theories the anisotropic stress is given by

$$\eta = \frac{F_{,\phi}^2}{F(\phi) + F_{,\phi}^2}, \quad (3.16)$$

and Eq. (3.15) implies that the quantities  $G_L$  and  $G_M$  are related via

$$G_L = \frac{1\eta + 2}{2\eta + 1} G_M. \quad (3.17)$$

In order to have agreement with the Solar System tests, viable models must satisfy  $F_{,\phi} \approx 0$  at  $z \approx 0$ , which from Eqs. (3.15) and (3.16) implies that  $\eta \approx 0$ . Similarly, from (3.17), we infer that at  $z \approx 0$ ,  $G_L \approx G_M \approx 1$  and  $\gamma_{\text{slip}} \approx 1$ .

Any of the above quantities  $G_M$ ,  $G_L$ ,  $\gamma_{\text{slip}}$ , or  $\eta$  can be used to construct a null test for GR. Alternative approaches like the growth index [95–102] can also be used for parametrizing deviations from GR. However, they are not as efficient in distinguishing the effects of the background  $H(z)$  from the effects of modified gravity since they do not enter explicitly in the dynamical growth equations.

In the present analysis, we focus on  $G_M = G_{\text{eff}}/G_N$  to parametrize deviations from GR since this is the only quantity that enters directly in the dynamical equation that determines the growth of density perturbations [Eq. (2.1)]. We thus use the parametrization

$$\begin{aligned} \frac{G_{\text{eff}}(a, n)}{G_N} &= 1 + g_a(1-a)^n - g_a(1-a)^{2n} \\ &= 1 + g_a \left( \frac{z}{1+z} \right)^n - g_a \left( \frac{z}{1+z} \right)^{2n}. \end{aligned} \quad (3.18)$$

Clearly, this parametrization mimics the large  $k$  limit of the above models, i.e., scales small compared to the horizon, which is a reasonable approximation even for large surveys. In addition, the parametrization (3.18) may be viewed as an extended Taylor expansion around  $a = 1$  for a fixed number of two parameters. The second term describes  $G_{\text{eff}}$  for low and intermediate values of  $z$ , while the third term describes  $G_{\text{eff}}$  for larger values of  $z$ . A similar parametrization concerning the dark energy equation of state was introduced in Ref. [103]. The parametrization (3.18) is only viable for  $n \geq 2$  due to the Solar System tests that demand that the first time derivative of  $G_{\text{eff}}$  should be zero.

However, at this point, it is important to mention that in the context of our analysis, we have assumed that the value of the effective Newton constant  $G_{\text{eff}}$  is independent of the presence of matter density. Thus, the value of  $G_{\text{eff}}$  on subhorizon scales is assumed to be scale and environment independent. We anticipate this assumption to be a good approximation in modified gravity models where in the physical frame there is no direct coupling of the scalar degree of freedom to matter density. In chameleon scalar-tensor field models, this assumption is not applicable, and therefore in such models, Solar System constraints are

much less stringent, and our parametrization with  $n = 1$  could be physically relevant. Therefore, in what follows, we will consider all values of  $n$  with  $n \geq 0$ .

Furthermore, this parametrization is motivated by considering that any viable modified gravity model must satisfy the following conditions:

- (i)  $G_{\text{eff}} > 0$  in order for the gravitons to carry positive energy.
- (ii)  $G_{\text{eff}}/G_N = 1.09 \pm 0.2$  to be in agreement with the big bang nucleosynthesis (BBN).
- (iii) Today, we should have  $G_{\text{eff}}(a = 1)/G_N = 1$  due to our choice for the normalization of  $F$ .

As can be seen then, for  $g_a > -4$ , our parametrization of Eq. (3.18) satisfies all of the aforementioned requirements.<sup>2</sup> One could also demand that at early times we have  $G'_{\text{eff}}(a = 0)/G_N = 1$ , i.e., we have GR, but that would require yet another term in Eq. (3.18), so that the coefficient can adjust the first derivative, but since the BBN constraint is not so stringent, we prefer to allow for some extra freedom in our model.

Another criterion we should take into account is the self-consistency of the modified gravity model, as not all parametrizations can be reproduced by a given model. For example, in Ref. [53], it was found that a scalar-tensor model cannot reproduce a given combination of  $G_{\text{eff}}(z)$  with  $H(z)$ . This was manifested by a negative kinetic term for the scalar field  $\Phi$ ; see Fig. 5 in Ref. [53].<sup>3</sup> Thus, we are lead to the following question: what are the allowed  $H(z) - G(z)$  regions for a given modified gravity model? For scalar-tensor theories and  $H(z)$  corresponding to  $\Lambda$ CDM, this question is addressed in the next section.

In the rest of this section, we fit the parametrization (3.18) to our Gold-2017, assuming a Planck15/ $\Lambda$ CDM background. The  $f\sigma_8$  data points of the Gold-2017 data set along with some model fits are shown in Fig. 2. The green dashed line corresponds to the best fit of the  $\Lambda$ CDM model ( $\chi^2 = 11.8$ ,  $\Omega_{0m} = 0.21$ ,  $\sigma_8 = 0.88$ ), the red dashed one corresponds to the Planck15/ $\Lambda$ CDM model parameter values ( $\chi^2 = 22.8$ ), and the blue dot-dashed one corresponds to the best fit of  $G_{\text{eff}}$  parametrization for ( $g_a = -1.16$ ,  $n = 2$ ) with the Planck15 background ( $\chi^2 = 13.5$ ). In particular, in Fig. 3, we show the 68.3%, 95.4%, and 99.7% confidence contours in the  $g_a$ - $n$  plane for  $n = 0$  and  $n = 2$ , while in Fig. 4, we show  $G_{\text{eff}}(a)$  for various values of  $n$  ( $n \in [2, 6]$ ) from the upper to the lower curve, respectively) and for  $g_a$  corresponding to the best-fit value. We note that for  $a \ll 1$  the constraint from BBN is satisfied since  $G_{\text{eff}}(a \ll 1)/G_N = 1$ .

<sup>2</sup>Note that for  $g_a < 0$  the parametrization of Eq. (3.18) has a minimum at  $a_{G_{\text{eff},\text{min}}} = 1 - 2^{-1/n}$  with a value of  $G_{\text{eff}}/G_N = 1 + \frac{g_a}{4}$ ; hence, in order to have  $G_{\text{eff}} > 0$ , we need  $g_a > -4$ , and as we will see later on, the best fit for various  $n$  satisfies that.

<sup>3</sup>For a similar reason, GR quintessence does not allow crossing of the phantom divide line  $w = -1$ , as this crossing would require a change of sign of the scalar field kinetic term.

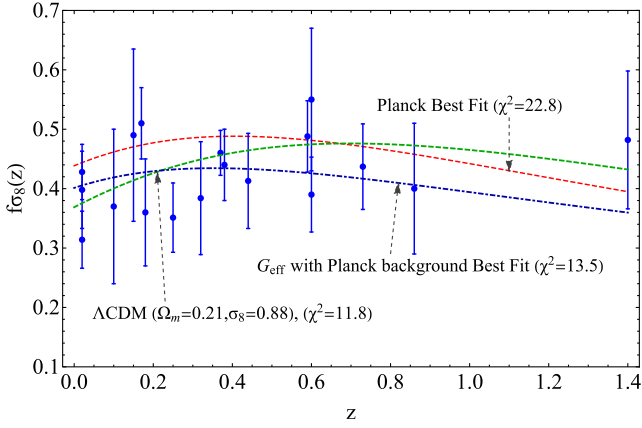


FIG. 2. Plot of  $f\sigma_8(z)$  for the Gold-2017 growth-rate data set. The green dashed line and the red dashed one correspond to the best fits of  $\Lambda$ CDM and Planck15/ $\Lambda$ CDM models, respectively, while the blue dot-dashed one corresponds to the best fit of  $G_{\text{eff}}$  parametrization for  $g_a = -1.16, n = 2$  with the Planck15 background.

Specifically, we explore systematically the parametric space for  $n = 1, 2, \dots, 6$ , while the best-fit values of  $g_a$  with error bars are shown explicitly in Table IV. It is important to mention at this point that these best-fit values refer to the first minimum of each  $\chi^2$ , which is not always the global one. We discuss the issue of the multiple minima in some detail in Appendix B. As can be seen from Fig. 3, this parametrization is capable of alleviating the tension found between the growth-rate data and the Planck15/ $\Lambda$ CDM best fit, reducing it from  $\sim 3\sigma$  to less than  $1\sigma$ , thus offering potential hints for new physics.

As mentioned above, the consistency of any modified gravity model with the Solar System tests is paramount as they place stringent constraints on the evolution of  $G_{\text{eff}}$ . Hence, viable models like the Hu and Sawicki model [92] that evade them are effectively small perturbations around the  $\Lambda$ CDM [see, e.g., Eq. (3.4)]. From a phenomenological point of view, it is also interesting to consider direct parametrizations of  $G_{\text{eff}}$  like the one of Eq. (3.18). Such

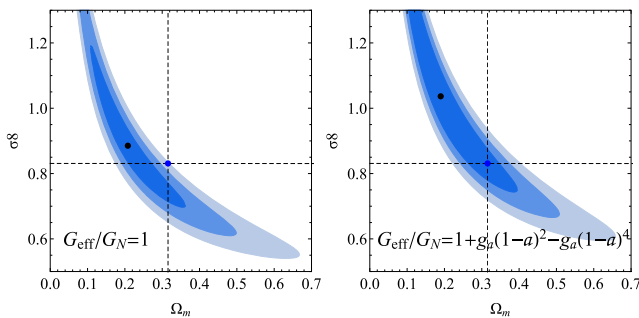


FIG. 3. The 68.3%, 95.4%, and 99.7% confidence contours in the  $g_a$ - $n$  plane for  $n = 0$  (left) and  $n = 2$  (right). In both cases, the point at the intersection of the dashed lines corresponds to the best-fit Planck15/ $\Lambda$ CDM model.

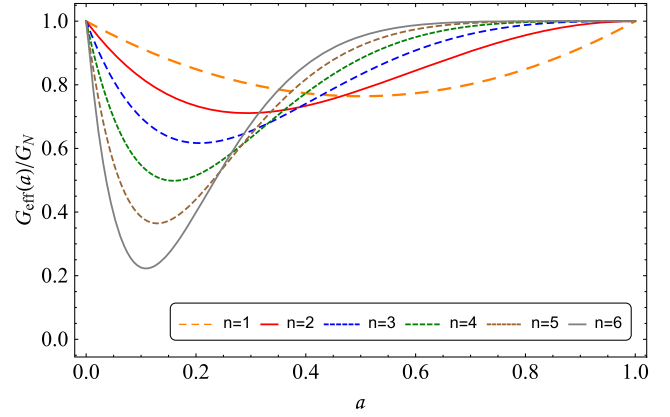


FIG. 4.  $G_{\text{eff}}(a)/G_N$  in the range  $n \in [1, 6]$  from the upper to lower curve, respectively, and for  $g_a$  corresponding to the best-fit value.

a consideration leads to the following question: are the best forms of  $G_{\text{eff}}$  able to lead to a reconstruction of self-consistent scalar-tensor quintessence with the Planck15/ $\Lambda$ CDM background? We will address this question in the next section.

#### IV. RECONSTRUCTION OF SCALAR-TENSOR QUINTESSENCE

The line element for the Friedmann-Lemaitre-Robertson-Walker (FLRW) metric corresponding to a flat universe is given by

$$ds^2 = -dt^2 + a^2(t)[dr^2 + r^2(d\theta^2 + \sin^2\theta d\phi^2)]. \quad (4.1)$$

Using this metric in the action (1.2) and assuming a homogeneous scalar field and a perfect fluid background, we find the dynamical equations of the system as

$$3FH^2 = \rho + \frac{1}{2}\dot{\phi}^2 - 3H\dot{F} + U \quad (4.2)$$

$$-2F\dot{H} = (\rho + p) + \dot{\phi}^2 + \ddot{F} - H\dot{F}. \quad (4.3)$$

TABLE IV. The best-fit values of  $g_a$  with errors bars for  $n = 1, 2, \dots, 6$ . As we describe in Appendix B, this parametrization has several distinct minima, but here we show only the global one when both  $g_a$  and  $n$  are free (first row) and then for integer values of  $n = 1, 2, \dots, 6$ , the minima corresponding to the lowest  $g_a$  which are also the global ones for low values of  $n$ .

$n$	$g_a$
0.343	$-1.200 \pm 1.025$
1	$-0.944 \pm 0.253$
2	$-1.156 \pm 0.341$
3	$-1.534 \pm 0.453$
4	$-2.006 \pm 0.538$
5	$-2.542 \pm 0.689$
6	$-3.110 \pm 0.771$

We eliminate the kinetic term  $\dot{\phi}^2$  in Eq. (4.3), and we set the squared rescaled Hubble parameter as

$$q(z) \equiv E^2(z) = \frac{H^2(z)}{H_0^2}, \quad (4.4)$$

while a new rescaling to potential is applied, i.e.,  $U \rightarrow U \cdot H_0^2$ . We thus obtain the dynamical equations in terms of the redshift  $z$  as

$$\begin{aligned} F''(z) + \left[ \frac{q'(z)}{2q(z)} - \frac{4}{1+z} \right] F'(z) \\ + \left[ \frac{6}{(1+z)^2} - \frac{2}{(1+z)} \frac{q'(z)}{2q(z)} \right] F \\ = \frac{2U(z)}{(1+z)^2 q(z)} + 3 \frac{1+z}{q(z)} \Omega_{0m} \end{aligned} \quad (4.5)$$

$$\phi'(z)^2 = -\frac{6F'(z)}{1+z} + \frac{6F(z)}{(1+z)^2} - \frac{2U(z)}{(1+z)^2 q(z)} - 6 \frac{1+z}{q(z)} \Omega_{0m}, \quad (4.6)$$

where the differentiation with respect to the redshift  $z$  is denoted by the prime and we have assumed a matter perfect fluid with  $p = 0$ ,  $\Omega_{0m} = 3\rho_{0m}/H_0^2$ . In addition, Eqs. (4.5) and (4.6) satisfy the initial conditions  $\phi(0) = 0$ ,  $F(0) = 1$ , and  $F'(0) = 0$  for consistency with Solar System tests ( $dF/d\phi \sim dF/dz \approx 0$  [56,104,105]).

In scalar-tensor theories, the effective Newton constant with respect to  $z$  is of the form (see Ref. [53])

$$G_{\text{eff}}(z) = \frac{1}{F} \frac{2F + 4\left(\frac{dF}{d\phi}\right)^2}{2F + 3\left(\frac{dF}{d\phi}\right)^2} G_{\text{N}} \simeq \frac{G_{\text{N}}}{F}, \quad (4.7)$$

where  $G_{\text{N}}$  is the well-known Newton constant in GR.

Equations (4.5) and (4.6) form the system of equations for  $\{U(z), \phi'(z)\}$  that can be used for the reconstruction of the theory [derivation of functions  $U(\phi)$ ,  $F(\phi)$ ], assuming that the functions  $F(z)$  [or  $G_{\text{eff}}(z)$ ] and  $H(z)$  are observationally obtained [87,106,107]. The function  $H(z)$  is well approximated by the Planck15/ $\Lambda$ CDM fit with parameters shown in Table I. The function  $G_{\text{eff}}(z)$  may be obtained using the growth data of Table III in the context of the parametrization (3.18) that satisfies the three basic conditions discussed in the previous section (Solar System tests, nucleosynthesis constraints, and proper normalization at the present time).

Even after the observational determination of  $G_{\text{eff}}(z)$  and  $H(z)$ , the self-consistent reconstruction of a modified theory is not always possible. For example, in the case of a scalar-tensor theory, the sign of  $\phi'(z)^2$  obtained from Eqs. (4.5) and (4.6) may turn out to be negative, leading to a complex predicted value of the scalar field. This violates that assumption of a real scalar field on which the theory is

based and leads to inconsistencies that may be difficult to overcome.

As shown in Fig. 4 and in Table IV, it is clear that the growth data indicate that the gravitational strength may be a decreasing function of the redshift in the redshift range  $[0, 0.4]$  compared to its present value. The question that we want to address is the following: can this weakening effect of gravity be due to an underlying scalar-tensor theory? If the answer is positive, then the sign of the reconstructed  $\phi'(z)^2$  should be positive so that the scalar field of the theory is real. We will show that a  $G_{\text{eff}}$  that is decreasing with redshift at low  $z$  is not consistent with positive  $\phi'(z)^2$ , and therefore this behavior cannot be due to an underlying scalar-tensor theory. This is shown numerically in Fig. 5 where we show the reconstructed form of  $\phi'(z)^2$  under the assumption of the best-fit forms of  $G_{\text{eff}}$  ( $n = 1, 2, 3, 4, 5, 6$ ) shown in Fig. 4 and the Planck15/ $\Lambda$ CDM background  $H(z)$  obtained with the parameters of Table I. Clearly, for all values of  $n$  considered,  $\phi'(z)^2$  is negative for low  $z$ , leading to an unacceptable scalar-tensor theory.

This result may be generalized analytically as follows: using Eqs. (4.5) and (4.6) and demanding that  $\phi'^2(z) \geq 0$ , we obtain

$$\begin{aligned} F''(z) + F'(z) \left( \frac{q'(z)}{2q(z)} + \frac{2}{z+1} \right) - F(z) \frac{q'(z)}{(z+1)q(z)} \\ + \frac{3\Omega_m(z+1)}{q(z)} \leq 0, \end{aligned} \quad (4.8)$$

which is a second-order differential inequality for  $F(z)$ .

A useful theorem for dealing with such inequalities is the Chaplygin theorem (see Ref. [108] and Appendix A for details). In order to bring the inequality (4.8) to the form required by the theorem, we first set  $F(z) = 1 - \delta f(z)$

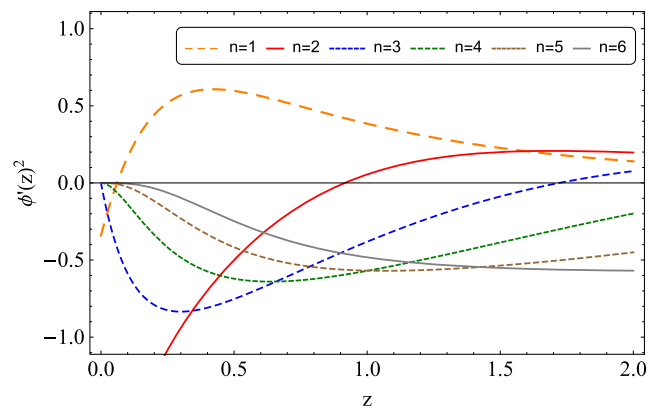


FIG. 5. The evolution with redshift of the kinetic term  $\phi'(z)^2$  for various values of  $n$  in the range  $z \in [0, 2]$ . Each case gives an imaginary scalar field which is not acceptable, leading to scalar-tensor theory inconsistencies. The line corresponding to  $n = 1$  is only applicable in a chameleon mechanism and thus is ruled out due to Solar System tests in the present analysis.

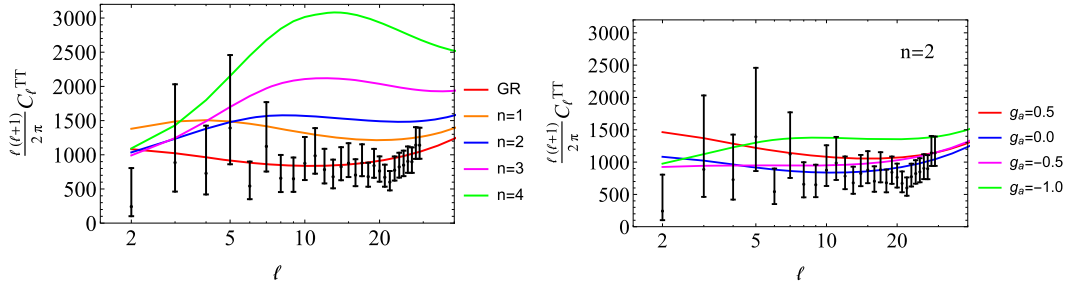


FIG. 6. The ISW effect for the  $G_{\text{eff}}$  model used in our analysis for various values of  $n$  evaluated at the minima for  $g_a$  given in Table IV (left) and for  $n = 2$  but for various values of  $g_a$  as indicated by the label. We also show the Planck15 low- $\ell$  binned  $C_\ell^{TT}$  data.

and deduce the corresponding inequality for  $\delta f(z)$ . We then find

$$\delta f''(z) + \delta f'(z) \left( \frac{2}{1+z} + \frac{q'(z)}{2q(z)} \right) - \delta f(z) \frac{q'(z)}{(1+z)q(z)} - \frac{3\Omega_m(1+z)}{q(z)} + \frac{q'(z)}{(1+z)q(z)} \geq 0. \quad (4.9)$$

By applying the theorem, as described in Appendix A, we find that the inequality (4.8) is satisfied for an  $\Lambda$ CDM background only when  $\delta f(z) \geq 0$  or  $F(z) \leq 1$  ( $G_{\text{eff}}(z)/G_N \geq 1$ ) for a range that includes all  $z \geq 0$ , as we found by a numerical analysis.

To summarize, in order to satisfy the inequality (4.8) along with the viability constraints (positive energy for the graviton, etc.) and to be able to reconstruct the scalar-tensor Lagrangian in a  $\Lambda$ CDM background, we need to have  $0 < F(z) \leq 1$  [ $G_{\text{eff}}(z)/G_N \geq 1$ ]. This result explains why the reconstruction as seen in Fig. 5 does not work. Every one of these cases has a negative value for  $\phi'(z)^2$  at some  $z$ , and as seen in Fig. 4, it also has  $F(z) > 1$  [ $G_{\text{eff}}(z)/G_N < 1$ ] in some region. Several numerical tests we performed with several models seem to corroborate the result of this theorem. This issue has also been discussed in Ref. [54] even though no general rule was derived for the viability of the reconstruction. Therefore, we conclude that the only viable models of scalar-tensor theories that can be reconstructed in the context of a  $\Lambda$ CDM background  $H(z)$  are the ones where the nonminimal coupling function satisfies  $0 < F(z) \leq 1$  for all  $z \geq 0$ . In the context of the reconstruction analysis, we have used the approximation that  $G_{\text{eff}} \approx \frac{1}{F}$ , which we find is valid everywhere except when  $\phi'(z)^2$  changes sign.

## V. EFFECTS OF $G_{\text{eff}}(z)$ ON THE CMB

In this section, we investigate the effects of a redshift-dependent  $G_{\text{eff}}(z)$  on the CMB spectrum. We anticipate (and verify with MGCAMB below) that  $G_{\text{eff}}(z)$  affects only the large angular CMB spectrum scales (low  $\ell$ ) through the integrated Sachs-Wolfe (ISW) effect while smaller scales (the acoustic peaks) depend only on the

background  $H(z)$  through the angular diameter distance  $d_A = \frac{c}{H_0} \frac{1}{1+z} \int_0^z \frac{1}{H(z')} dz'$ . The ISW effect is significantly affected by the redshift dependence of  $G_{\text{eff}}$  because it depends on the time evolution of the potential  $\Phi(z)$  which in turn depends on  $G_{\text{eff}}$  due to the Poisson equation  $\frac{k^2}{a^2} \Phi(k, z) \propto \delta(z) \cdot G_{\text{eff}}(k, z)$ , where  $\delta = \frac{\delta\rho}{\rho}$  is the growth factor.

In Fig. 6, we show a comparison of the theoretically predicted low- $\ell$  multipoles of the Temperature-Temperature (TT) part of the CMB spectrum including the ISW effect for the best-fit  $G_{\text{eff}}$  models (Table IV) (continuous lines, left panel). The Planck15 low- $\ell$  binned  $C_\ell^{TT}$  data are also shown. The theoretically predicted spectra were obtained with a modified version of MGCAMB [109] with  $G_{\text{eff}}(z)/G_N$  given by (3.18), anisotropic stress  $\eta(z) = 0$ , and with the parameter values shown in Table IV for  $n = 2, 3, 4$  and for  $G_{\text{eff}}/G_N = 1$  for GR. The right panel of Fig. 6 shows the theoretically predicted CMB spectra for  $n = 2$  and various values of  $g_a$ .

Clearly, the higher the exponent  $n$  of our parametrization for  $G_{\text{eff}}$ , the stronger the ISW effect and its deviation from the  $\Lambda$ CDM model. Thus, the cases for  $n = 5, 6$  are not included in Fig. 6 as they are not consistent with the observed CMB power spectrum. As shown in Fig. 4, a higher  $n$  means that gravitational strength varies more rapidly at low  $z$ , leading to the stronger ISW effect shown in Fig. 6.

Also, we performed a simple  $\chi^2$  analysis with the low- $\ell$  data, where we defined

$$\chi_{\text{low-}\ell}^2 = \sum_{i=1}^N \left( \frac{D_\ell^{\text{Pl}} - D_\ell^{\text{th}}}{\sigma_{D_\ell^{\text{Pl}}}} \right)^2 \quad (5.1)$$

and  $D_\ell = \frac{\ell(\ell+1)}{2\pi} C_\ell^{TT}$ . In this case, we kept all other parameters except  $g_a$  and  $n$  fixed to their Planck15/ $\Lambda$ CDM values. We found that the  $\Lambda$ CDM model ( $n = 0$  or  $g_a = 0$ ) has  $\chi_{GR}^2 = 22.394$  and the rest of the models have  $\chi_{n=2}^2 = 255.683$ ,  $\chi_{n=3}^2 = 723.922$ , and  $\chi_{n=4}^2 = 2086.69$ . Thus, these models are strongly disfavored with respect to  $\Lambda$ CDM due to their rapid variation of  $G_{\text{eff}}$  leading to strong effects on the ISW effect. In the case of fixed  $n$ , we find that

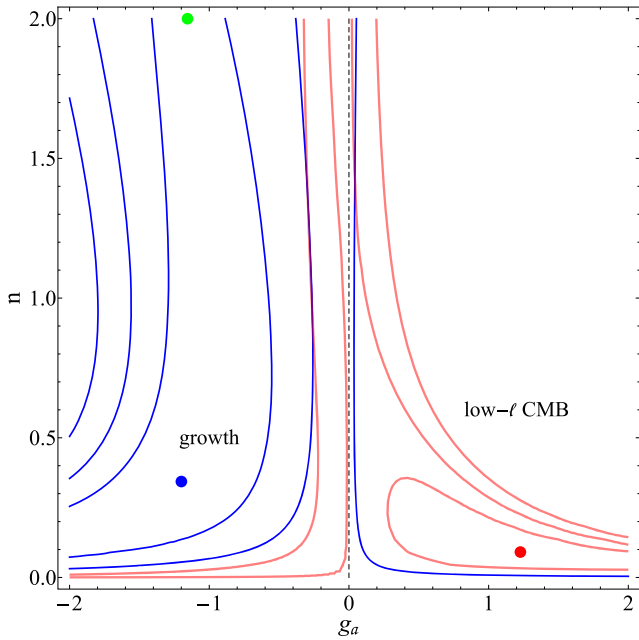


FIG. 7. The  $1\sigma$ ,  $2\sigma$ , and  $3\sigma$  contours for the  $G_{\text{eff}}$  model in the  $(g_a, n)$  parameter space based on the low- $\ell$ TT CMB data (red lines) and the growth-rate data (blue lines). The black dashed line at  $g_a = 0$  and also the axis at  $n = 0$  correspond to GR and the  $\Lambda$ CDM model, while the green, blue, and red dots correspond to the best fit for  $n = 2$ , i.e.,  $(g_a, n) = (-1.156, 2)$ ; the global minimum for  $(g_a, n) = (-1.200, 0.343)$ ; and the minimum for the low- $\ell$  data, i.e.,  $(g_a, n) = (1.227, 0.091)$ , respectively. The blue and red contour regions are centered around the blue and red points, respectively. As can be seen, there is a strong tension between the two data sets.

$\chi^2_{g_a=0.5} = 66.346$ ,  $\chi^2_{g_a=0} = 22.394$ ,  $\chi^2_{g_a=-0.5} = 42.755$ , and  $\chi^2_{g_a=-1} = 186.969$ , or in the case of  $g_a = -0.5$ ,  $\delta\chi^2 = 20.361$ , corresponding to a  $4.1\sigma$  deviation. Thus, the ISW effect provides significantly stronger constraints on  $G_{\text{eff}}(z)$  than the growth data.

Our assumption that the probability distribution of the low- $\ell$ TT CMB spectrum likelihood can be modeled as a Gaussian may not be accurate (see Ref. [110]) and can introduce additional uncertainties which may reduce the

tension level found in our analysis. Therefore, our  $\chi^2$  analysis with the low- $\ell$ TT CMB data should be interpreted with extreme caution as it neglects the covariances of the data but also possible effects from the foregrounds which are clearly non-Gaussian. The effect of the non-Gaussianity will manifest itself as higher-order terms related to the skewness and the kurtosis, which has been shown to be relevant for the CMB (see, e.g., Ref. [111]).

In Fig. 7, we also show the contours for the  $G_{\text{eff}}$  model in the  $(g_a, n)$  parameter space based on the low- $\ell$ TT CMB data (red lines) and the growth-rate data (blue lines). The black dashed line at  $g_a = 0$  and the axis at  $n = 0$  correspond to GR and the  $\Lambda$ CDM model since the last two terms in (3.18) in both cases cancel out. The green, blue, and red dots correspond to the best fit for  $n = 2$ , i.e.,  $(g_a, n) = (-1.156, 2)$ ; the global minimum for  $(g_a, n) = (-1.200, 0.343)$ ; and the minimum for the low- $\ell$  data, i.e.,  $(g_a, n) = (1.227, 0.091)$ , respectively. Clearly, there is strong tension between the best-fit growth data and the Planck low- $\ell$  power spectrum (ISW effect).

Another interesting probe to consider is the CMB lensing [112] which is sensitive to the impact of a modified growth rate. Clearly, modifications introduced by a time-dependent gravitational constant translate to significant changes in the CMB lensing. In this regard, in Fig. 8, we show the lensing potential for Planck15- $\Lambda$ CDM (black solid line) along with the  $G_{\text{eff}}$  model for  $g_a = \pm 0.1$  (black dashed line) and  $g_a = \pm 0.2$  (blue dot-dashed line). The data points are from Planck 2015 and were derived from the observed trispectrum [112].

By fitting the modified lensing potentials for  $\Lambda$ CDM to the data, we have also obtained new stronger constraints on the parameters of our parametrization. In Fig. 9, we show the  $1\sigma$ ,  $2\sigma$ , and  $3\sigma$  contours for the  $G_{\text{eff}}$  model in the  $(g_a, n)$  parameter space based on the CMB lensing (trispectrum [112]) data (red contours) and the growth-rate data (blue lines). The black dashed line at  $g_a = 0$  and also the axis at  $n = 0$  correspond to GR and the  $\Lambda$ CDM model, while the green and blue points correspond to the best fit for  $n = 2$ , i.e.,  $(g_a, n) = (-1.156, 2.000)$  and the global minimum for  $(g_a, n) = (-1.200, 0.343)$  with the growth-rate data, while the black point to the CMB lensing best fit for

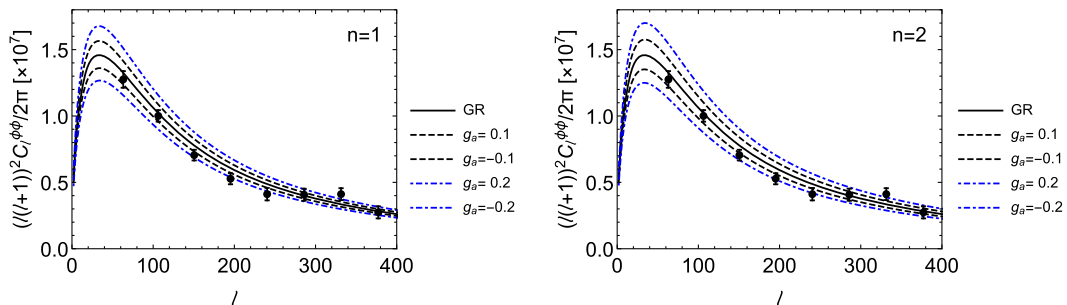


FIG. 8. The lensing potential for  $\Lambda$ CDM (black solid line) or the  $G_{\text{eff}}$  model for  $g_a = \pm 0.1$  (black dashed line) and  $g_a = \pm 0.2$  (blue dot-dashed line). The data points are from Planck 2015 and were derived from the observed trispectrum [112].

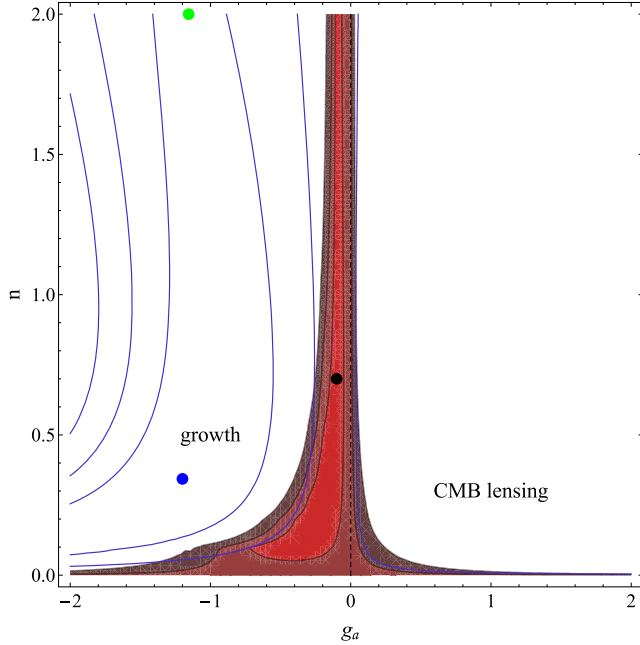


FIG. 9. The  $1\sigma$ ,  $2\sigma$ , and  $3\sigma$  contours for the  $G_{\text{eff}}$  model in the  $(g_a, n)$  parameter space based on the CMB lensing (trispectrum [112]) data (red contours) and the growth-rate data (blue lines). The black dashed line at  $g_a = 0$  and also the axis at  $n = 0$  correspond to GR and the  $\Lambda$ CDM model, while the green and blue points correspond to the best fit for  $n = 2$ , i.e.,  $(g_a, n) = (-1.156, 2.000)$  and the global minimum for  $(g_a, n) = (-1.200, 0.343)$  with the growth-rate data, while the black point to the CMB lensing best fit for  $(g_a, n) = (-0.200, 0.700)$ . As can be seen, there is a mild  $2\sigma$  tension between the growth data contours (blue lines) and the CMB lensing contours (red lines).

$(g_a, n) = (-0.200, 0.700)$ . As can be seen, there is a mild  $2\sigma$  tension, and the allowed parameter space from the lensing potential data is significantly reduced and much more constraining than the ISW.

Finally, as mentioned above, the  $\chi^2$  analysis with the low- $\ell$ TT CMB data should be interpreted with extreme caution as it neglects the covariances and the non-Gaussianity of the data [110]. In addition all other parameters, such as  $\Omega_m, H_0$ , etc., are fixed to their Planck15/ $\Lambda$ CDM values, so it would be worthwhile to do a full Markov Chain Monte Carlo (MCMC) and explore the whole parameter space, which is left for future work. Thus, our analysis indicates that, even though the tension between the growth data and the Planck15/ $\Lambda$ CDM background in the context of GR is removed by allowing a redshift evolution of  $G_{\text{eff}}(z)$ , the required  $G_{\text{eff}}(z)$  is not consistent with either scalar-tensor theories nor the low- $\ell$  CMB spectrum as determined by the ISW effect.

## VI. CONCLUSIONS AND DISCUSSION

We presented a collection of 34 growth-rate data based on recent RSD measurements obtained from several

surveys and studies over the last ten years. In an effort to maximize robustness and independence of the data, we selected 18 of the 34 growth-rate data to construct a Gold-2017 growth-rate data set. Using this data set, we fit a  $w$ CDM cosmology and find that the best-fit parameters  $(w, \sigma_8, \Omega_{0m})$  are in  $3\sigma$  tension with the corresponding parameters obtained with the Planck15 CMB data in the context of GR and  $\Lambda$ CDM. In order to resolve this tension, we consider a simple parametrization for  $G_{\text{eff}}$  given by Eq. (3.18). We show that the tension in the parameters of the data gets now reduced to the  $1\sigma$  level.

Despite this reduction of the tension between the growth data and the Planck indicated background, this best-fit parametrization of  $G_{\text{eff}}(z)$  was shown to have two important problems:

- (1) It is a decreasing function of the redshift, and therefore according to a general rule, the validity of which we demonstrated, it cannot be supported by a self-consistent scalar-tensor theory because it leads to a negative scalar field kinetic term.
- (2) It predicts a large ISW effect that is not consistent with the observed large scale (low- $\ell$ ) CMB spectrum.

These problems could potentially be resolved by considering more general modified gravity models which can potentially support the derived best-fit  $G_{\text{eff}}(z)$  such as Horndeski models [113–115] or bimetric gravity [116]. The tension of the best-fit  $G_{\text{eff}}(z)$  with the low- $\ell$  CMB spectrum induced by the ISW effect is more difficult to resolve and may indicate either required modifications on the background Planck15/ $\Lambda$ CDM  $H(z)$  or systematics in the growth data.

The strategy of our analysis has been the identification of the consistency (or tension) of the Planck15/ $\Lambda$ CDM model with the growth data. In the context of this goal, we have chosen to fix the  $\Lambda$ CDM parameters to the Planck15 values. Clearly, the level of the tension can be reduced significantly if we vary the  $\Lambda$ CDM parameters, and in fact, it may completely disappear if we consider background  $H(z)$  parametrizations beyond  $\Lambda$ CDM. However, such an approach would not be consistent with the above-described strategy.

We have pointed out the need for the construction of optimized, large, self-consistent compilations of the emerging growth data and have made a first attempt in that direction. Our updated Gold-2017 data set compilation comes from reliable sources, i.e., major surveys and international collaborations. However, the fact that it consists of only a small amount of points indicates that there is significant potential for improvement. This situation will definitely improve in the coming decade as the Euclid [51] and LSST [52] surveys will release a significant amount of new high quality data points, and as a result, very soon we will be able to detect any possible deviations from GR with a high level of confidence.

### ACKNOWLEDGMENTS

The authors thank Judit Perez for pointing out a couple of minor typographical errors. S. N. acknowledges support from the Research Project of the Spanish MINECO, Project No. FPA2013-47986-03-3P; the Centro de Excelencia Severo Ochoa Program No. SEV-2012-0249; and the Ramón y Cajal program through Grant No. RYC-2014-15843.

### APPENDIX A: CHAPLYGIN THEOREM

The Chaplygin theorem [108] states that if  $y(x)$  satisfies the  $n$ th-order differential inequality

$$L[y] \equiv y^n(x) + a_1(x)y^{n-1}(x) + \dots + a_n(x) > b(x), \quad (\text{A1})$$

where the  $a_n(x)$  can be integrated and the function  $f(x)$  satisfies the differential equation

$$L(f) = b(x) \quad (\text{A2})$$

with the same initial conditions as Eq. (A1), i.e.,  $f(x_0) = y(x_0), \dots, f^{n-1}(x_0) = y^{n-1}(x_0)$ , then there is a region  $x \in (x_0, x_*)$  such that  $y(x) > f(x)$  and  $x_*$  is specified by the region for which for every  $\xi \in [x_0, x]$  we have  $G(s, \xi) \geq 0$ , where  $G$  satisfies the Green equation with initial conditions

$$L[G] = 0$$

$$G(x = \xi) = \dots = G^{n-2}(x = \xi) = 0, G^{n-1}(x = \xi) = 1.$$

By specifying the region where  $G \geq 0$ , we can thus determine where  $y(x) > f(x)$ .

### APPENDIX B: MULTIPLE MINIMA

A rather interesting feature that arises by minimizing the  $\chi^2$  of the Gold-2017 data set using the  $G_{\text{eff}}$  parametrization (3.18) is the one of the multiple minima (see Ref. [117]). Specifically, as the number of  $n$  increases the more minima we observe. This effect is due to the fact that the solution of the growth-rate ordinary differential equation (ODE) of Eq. (2.1) contains Bessel functions which have degeneracies in their arguments. In order to keep things simple, we will now consider a toy model with  $\Omega_m = 1$  and

$G_{\text{eff}}/G_N = 1 + g_n(1 - a)^n$ , even though this model does not satisfy the viability criteria described in the text. Then, for  $n = 1$  and  $\Omega_m = 1$ , the solution to the differential equation (2.1) is

$$\delta_{n=1}(a) = c_1 a^{-1/4} J_m(\sqrt{6ag_n}) + c_2 a^{-1/4} J_{-m}(\sqrt{6ag_n}), \quad (\text{B1})$$

while for  $n = 2$ , we have

$$\delta_{n=2}(a) = e^{-\frac{1}{2}\beta a} a^{\frac{m}{2}-\frac{1}{4}} \left( c_1 U\left(\frac{1}{2}(m - \beta + 1), m + 1, a\beta\right) + c_2 L_{\frac{1}{2}(\beta-m-1)}^m(a\beta) \right), \quad (\text{B2})$$

where  $c_{1,2}$  are constants to be determined for the growing and decaying mode and  $m = \frac{1}{2}\sqrt{24g_n + 25}$ ,  $\beta = \sqrt{6g_n}$  and  $J_{\pm m}(z)$ ,  $U(\kappa_1, \kappa_2, z)$  and  $L_n^\kappa$  are the BesselJ, the confluent hypergeometric  $U$ , and the Laguerre-L functions, respectively. As can be seen in this case, the presence of these functions in the solution of the growth rate is the root cause of the multiple minima since the variable  $g_n$  of the model appears both in the order and the argument of the functions. As a result, the growth will be degenerate with respect to  $g_n$ , i.e., for many different values of  $g_n$ , we will have the same growth factor. Similar arguments can be made for any value of  $\Omega_m$ , since the case studied here ( $\Omega_m = 1$ ) is just a limit of the  $\Lambda$ CDM model. The same also applies to other similar  $G_{\text{eff}}$  models, besides the one used in the main analysis.

Note that the first minimum is not always the global one, i.e., the minimum with the smallest value of  $\chi^2$ . In Fig. 10, we show the  $\chi^2(g_n)$  plot corresponding to our parametrization (3.18) for  $n = 2, 3, 4$ , where for  $n = 2, 3$  the first minimum is the global one; e.g., for  $n = 3$ , the first minimum corresponds to ( $\chi^2 = 14.3, g_n = -1.534$ ), while the second one corresponds to ( $\chi^2 = 14.6, g_n = -11.14$ ). On the other hand, for  $n = 4$ , the first three minima from right to left correspond to ( $\chi^2 = 14.9, g_n = -2.006$ ), ( $\chi^2 = 12.6, g_n = -10.56$ ), and ( $\chi^2 = 14.8, g_n = -21.87$ ), respectively, and therefore the global minimum is the second one (albeit with a small difference). However, since  $g_n$  must be small, we consider only the first minimum, which for small values of  $n$  is the global one as well.

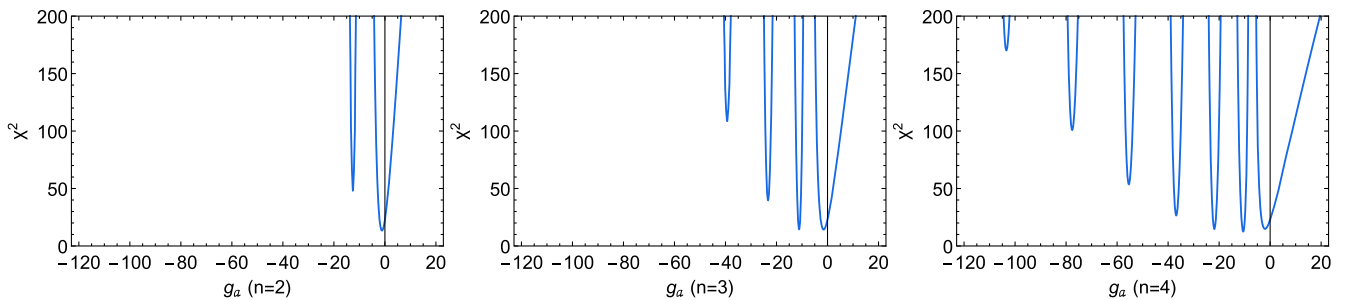


FIG. 10. Plots of the  $\chi^2(g_a)$  for  $n = 2, 3, 4$  that clearly show the degeneracy of the model and the many minima of the  $\chi^2$  in terms of  $g_a$ .

- [1] P. Bull *et al.*, Beyond  $\Lambda$ CDM: Problems, solutions, and the road ahead, *Phys. Dark Universe* **12**, 56 (2016).
- [2] S. Tsujikawa, *Dark energy: Investigation and modeling*, Astrophysics and Space Science Library Vol. 370 (Springer, Netherlands, 2011), pp. 331–402.
- [3] R. R. Caldwell and M. Kamionkowski, The physics of cosmic acceleration, *Annu. Rev. Nucl. Part. Sci.* **59**, 397 (2009).
- [4] E. J. Copeland, M. Sami, and S. Tsujikawa, Dynamics of dark energy, *Int. J. Mod. Phys. D* **15**, 1753 (2006).
- [5] P. A. R. Ade *et al.* (Planck Collaboration), Planck 2015 results. XIII. Cosmological parameters, *Astron. Astrophys.* **594**, A13 (2016).
- [6] G. Hinshaw *et al.* (WMAP Collaboration), Nine-Year Wilkinson Microwave Anisotropy Probe (WMAP) observations: Cosmological parameter results, *Astrophys. J. Suppl. Ser.* **208**, 19 (2013).
- [7] R. Watkins and H. A. Feldman, Large-scale bulk flows from the Cosmicflows-2 catalogue, *Mon. Not. R. Astron. Soc.* **447**, 132 (2015).
- [8] É. Aubourg *et al.*, Cosmological implications of baryon acoustic oscillation measurements, *Phys. Rev. D* **92**, 123516 (2015).
- [9] T. Delubac *et al.* (BOSS Collaboration), Baryon acoustic oscillations in the Ly-alpha forest of BOSS DR11 quasars, *Astron. Astrophys.* **574**, A59 (2015).
- [10] M. Betoule *et al.* (SDSS Collaboration), Improved cosmological constraints from a joint analysis of the SDSS-II and SNLS supernova samples, *Astron. Astrophys.* **568**, A22 (2014).
- [11] D. Huterer *et al.*, Growth of cosmic structure: Probing dark energy beyond expansion, *Astropart. Phys.* **63**, 23 (2015).
- [12] S. Nesseris and D. Sapone, Accuracy of the growth index in the presence of dark energy perturbations, *Phys. Rev. D* **92**, 023013 (2015).
- [13] S. Basilakos and A. Pouri, The growth index of matter perturbations and modified gravity, *Mon. Not. R. Astron. Soc.* **423**, 3761 (2012).
- [14] S. Nesseris and L. Perivolaropoulos, Testing Lambda CDM with the growth function  $\delta(a)$ : Current constraints, *Phys. Rev. D* **77**, 023504 (2008).
- [15] L. Izzo, M. Muccino, E. Zaninoni, L. Amati, and M. Della Valle, New measurements of  $\Omega_m$  from gamma-ray bursts, *Astron. Astrophys.* **582**, A115 (2015).
- [16] J.-J. Wei, X.-F. Wu, and F. Melia, The gamma-ray burst Hubble diagram and its implications for cosmology, *Astrophys. J.* **772**, 43 (2013).
- [17] L. Samushia and B. Ratra, Constraining dark energy with gamma-ray bursts, *Astrophys. J.* **714**, 1347 (2010).
- [18] E. J. Baxter *et al.* (DES and SPT Collaborations), Joint measurement of lensing-galaxy correlations using SPT and DES SV data, *Mon. Not. R. Astron. Soc.* **461**, 4099 (2016).
- [19] X. Ding, M. Biesiada, S. Cao, Z. Li, and Z.-H. Zhu, Is there evidence for dark energy evolution?, *Astrophys. J.* **803**, L22 (2015).
- [20] R. Chávez, M. Plionis, S. Basilakos, R. Terlevich, E. Terlevich, J. Melnick, F. Bresolin, and A. L. González-Morán, Constraining the dark energy equation of state with HII galaxies, *Mon. Not. R. Astron. Soc.* **462**, 2431 (2016).
- [21] S. W. Allen, D. A. Rapetti, R. W. Schmidt, H. Ebeling, G. Morris, and A. C. Fabian, Improved constraints on dark energy from Chandra X-ray observations of the largest relaxed galaxy clusters, *Mon. Not. R. Astron. Soc.* **383**, 879 (2008).
- [22] A. Morandi and M. Sun, Probing dark energy via galaxy cluster outskirts, *Mon. Not. R. Astron. Soc.* **457**, 3266 (2016).
- [23] M. Raveri, Are cosmological data sets consistent with each other within the  $\Lambda$  cold dark matter model?, *Phys. Rev. D* **93**, 043522 (2016).
- [24] J. Luis Bernal, L. Verde, and A. G. Riess, The trouble with  $H_0$ , *J. Cosmol. Astropart. Phys.* **10** (2016) 019.
- [25] B. F. Roukema, P. Mourier, T. Buchert, and J. J. Ostrowski, The background Friedmannian Hubble constant in relativistic inhomogeneous cosmology and the age of the Universe, *Astron. Astrophys.* **598**, A111 (2017).
- [26] E. Abdalla, E. G. M. Ferreira, J. Quintin, and B. Wang, New evidence for interacting dark energy from BOSS, *Phys. Rev. D* **95**, 043520 (2017).
- [27] X. -Lei Meng, X. Wang, S.-Y. Li, and T.-J. Zhang, Utility of observational Hubble parameter data on dark energy evolution, [arXiv:1507.02517](https://arxiv.org/abs/1507.02517).
- [28] Q.-G. Huang and K. Wang, How the dark energy can reconcile Planck with local determination of the Hubble constant, *Eur. Phys. J. C* **76**, 506 (2016).
- [29] J. Sola, A. Gomez-Valent, and J. de Cruz Pérez, First evidence of running cosmic vacuum: challenging the concordance model, *Astrophys. J.* **836**, 43 (2017).
- [30] J. Sola, J. de Cruz Perez, and A. Gomez-Valent, Towards the firsts compelling signs of vacuum dynamics in modern cosmological observations, [arXiv:1703.08218](https://arxiv.org/abs/1703.08218).
- [31] Q. Gao and Y. Gong, The tension on the cosmological parameters from different observational data, *Classical Quantum Gravity* **31**, 105007 (2014).
- [32] S. Perlmutter *et al.* (Supernova Cosmology Project Collaboration), Measurements of Omega and Lambda from 42 high redshift supernovae, *Astrophys. J.* **517**, 565 (1999).
- [33] A. G. Riess *et al.* (Supernova Search Team Collaboration), Observational evidence from supernovae for an accelerating universe and a cosmological constant, *Astron. J.* **116**, 1009 (1998).
- [34] G. Efstathiou, W. J. Sutherland, and S. J. Maddox, The cosmological constant and cold dark matter, *Nature (London)* **348**, 705 (1990).
- [35] L. Moscardini, S. Borgani, P. Coles, F. Lucchin, S. Matarrese, A. Messina, and M. Plionis, Large scale angular correlations in CDM models, *Astrophys. J.* **413**, L55 (1993).
- [36] K. M. Gorski, J. Silk, and N. Vittorio, Cold Dark Matter Confronts the Cosmic Microwave Background: Large Angular Scalar Anisotropies in Omega0 + lambda = 1 Models, *Phys. Rev. Lett.* **68**, 733 (1992).
- [37] B. Ratra and P. J. E. Peebles, CDM cosmogony in an open universe, *Astrophys. J.* **432**, L5 (1994).
- [38] L. A. Kofman, N. Y. Gnedin, and N. A. Bahcall, Cosmological constant, COBE cosmic microwave background anisotropy, and large scale clustering, *Astrophys. J.* **413**, 1 (1993).

- [39] L. M. Krauss and M. S. Turner, The cosmological constant is back, *Gen. Relativ. Gravit.* **27**, 1137 (1995).
- [40] C. Heymans *et al.*, CFHTLenS tomographic weak lensing cosmological parameter constraints: Mitigating the impact of intrinsic galaxy alignments, *Mon. Not. R. Astron. Soc.* **432**, 2433 (2013).
- [41] P. A. R. Ade *et al.* (Planck Collaboration), Planck 2013 results. XX. Cosmology from Sunyaev-Zeldovich cluster counts, *Astron. Astrophys.* **571**, A20 (2014).
- [42] E. Macaulay, I. K. Wehus, and H. K. Eriksen, Lower Growth Rate from Recent Redshift Space Distortion Measurements than Expected from Planck, *Phys. Rev. Lett.* **111**, 161301 (2013).
- [43] S. Alam *et al.* (BOSS Collaboration), The clustering of galaxies in the completed SDSS-III Baryon Oscillation Spectroscopic Survey: cosmological analysis of the DR12 galaxy sample, [arXiv:1607.03155](https://arxiv.org/abs/1607.03155).
- [44] N. MacCrann, J. Zuntz, S. Bridle, B. Jain, and M. R. Becker, Cosmic discordance: Are Planck CMB and CFHTLenS weak lensing measurements out of tune?, *Mon. Not. R. Astron. Soc.* **451**, 2877 (2015).
- [45] R. A. Battye, T. Charnock, and A. Moss, Tension between the power spectrum of density perturbations measured on large and small scales, *Phys. Rev. D* **91**, 103508 (2015).
- [46] T. D. Kitching, L. Verde, A. F. Heavens, and R. Jimenez, Discrepancies between CFHTLenS cosmic shear and Planck: New physics or systematic effects?, *Mon. Not. R. Astron. Soc.* **459**, 971 (2016).
- [47] J. Hamann and J. Hasenkamp, A new life for sterile neutrinos: resolving inconsistencies using hot dark matter, *J. Cosmol. Astropart. Phys.* **10** (2013) 044.
- [48] M. Kunz, S. Nesseris, and I. Sawicki, Using dark energy to suppress power at small scales, *Phys. Rev. D* **92**, 063006 (2015).
- [49] E.-M. Mueller, W. Percival, E. Linder, S. Alam, G.-B. Zhao, A. G. Sánchez, and F. Beutler, The clustering of galaxies in the completed SDSS-III Baryon Oscillation Spectroscopic Survey: constraining modified gravity, [arXiv:1612.00812](https://arxiv.org/abs/1612.00812).
- [50] N. Kaiser, Clustering in real space and in redshift space, *Mon. Not. R. Astron. Soc.* **227**, 1 (1987).
- [51] L. Amendola *et al.*, Cosmology and fundamental physics with the euclid satellite, [arXiv:1606.00180](https://arxiv.org/abs/1606.00180).
- [52] Paul A. Abell *et al.* (LSST Science and LSST Project Collaborations), LSST Science Book, Version 2.0, [arXiv:0912.0201](https://arxiv.org/abs/0912.0201).
- [53] S. Nesseris and L. Perivolaropoulos, Evolving newton's constant, extended gravity theories and snia data analysis, *Phys. Rev. D* **73**, 103511 (2006).
- [54] G. Esposito-Farese and D. Polarski, Scalar tensor gravity in an accelerating universe, *Phys. Rev. D* **63**, 063504 (2001).
- [55] F. Perrotta, C. Baccigalupi, and S. Matarrese, Extended quintessence, *Phys. Rev. D* **61**, 023507 (1999).
- [56] C. M. Will, The Confrontation between general relativity and experiment, *Living Rev. Relativ.* **9**, 3 (2006).
- [57] B. Boisseau, G. Esposito-Farese, D. Polarski, and A. A. Starobinsky, Reconstruction of a Scalar Tensor Theory of Gravity in an Accelerating Universe, *Phys. Rev. Lett.* **85**, 2236 (2000).
- [58] Y.-S. Song and W. J. Percival, Reconstructing the history of structure formation using Redshift Distortions, *J. Cosmol. Astropart. Phys.* **10** (2009) 004.
- [59] M. Davis, A. Nusser, K. Masters, C. Springob, J. P. Huchra, and G. Lemson, Local gravity versus local velocity: Solutions for  $\beta$  and nonlinear bias, *Mon. Not. R. Astron. Soc.* **413**, 2906 (2011).
- [60] M. J. Hudson and S. J. Turnbull, The growth rate of cosmic structure from peculiar velocities at low and high redshifts, *Astrophys. J.* **751**, L30 (2012).
- [61] S. J. Turnbull, M. J. Hudson, H. A. Feldman, M. Hicken, R. P. Kirshner, and R. Watkins, Cosmic flows in the nearby universe from Type Ia Supernovae, *Mon. Not. R. Astron. Soc.* **420**, 447 (2012).
- [62] L. Samushia, W. J. Percival, and A. Raccanelli, Interpreting large-scale redshift-space distortion measurements, *Mon. Not. R. Astron. Soc.* **420**, 2102 (2012).
- [63] C. Blake *et al.*, The WiggleZ Dark Energy Survey: Joint measurements of the expansion and growth history at  $z < 1$ , *Mon. Not. R. Astron. Soc.* **425**, 405 (2012).
- [64] R. Tojeiro *et al.*, The clustering of galaxies in the SDSS-III Baryon Oscillation Spectroscopic Survey: measuring structure growth using passive galaxies, *Mon. Not. R. Astron. Soc.* **424**, 2339 (2012).
- [65] C.-H. Chuang and Y. Wang, Modeling the anisotropic two-point galaxy correlation function on small scales and improved measurements of  $H(z)$ ,  $D_A(z)$ , and  $\beta(z)$  from the Sloan Digital Sky Survey DR7 luminous red galaxies, *Mon. Not. R. Astron. Soc.* **435**, 255 (2013).
- [66] F. Beutler, C. Blake, M. Colless, D. Heath Jones, L. Staveley-Smith, G. B. Poole, L. Campbell, Q. Parker, W. Saunders, and F. Watson, The 6dF Galaxy Survey:  $z \approx 0$  measurement of the growth rate and  $\sigma_8$ , *Mon. Not. R. Astron. Soc.* **423**, 3430 (2012).
- [67] C. Blake *et al.*, Galaxy And Mass Assembly (GAMA): Improved cosmic growth measurements using multiple tracers of large-scale structure, *Mon. Not. R. Astron. Soc.* **436**, 3089 (2013).
- [68] A. G. Sanchez *et al.*, The clustering of galaxies in the SDSS-III Baryon Oscillation Spectroscopic Survey: cosmological implications of the full shape of the clustering wedges in the data release 10 and 11 galaxy samples, *Mon. Not. R. Astron. Soc.* **440**, 2692 (2014).
- [69] C.-H. Chuang *et al.*, The clustering of galaxies in the SDSS-III Baryon Oscillation Spectroscopic Survey: single-probe measurements from CMASS anisotropic galaxy clustering, *Mon. Not. R. Astron. Soc.* **461**, 3781 (2016).
- [70] S. de la Torre *et al.*, The VIMOS Public Extragalactic Redshift Survey (VIPERS). Galaxy clustering and redshift-space distortions at  $z = 0.8$  in the first data release, *Astron. Astrophys.* **557**, A54 (2013).
- [71] C. Howlett, A. Ross, L. Samushia, W. Percival, and M. Manera, The clustering of the SDSS main galaxy sample—II. Mock galaxy catalogues and a measurement of the growth of structure from redshift space distortions at  $z = 0.15$ , *Mon. Not. R. Astron. Soc.* **449**, 848 (2015).
- [72] M. Feix, A. Nusser, and E. Branchini, Growth Rate of Cosmological Perturbations at  $z \sim 0.1$  from a New Observational Test, *Phys. Rev. Lett.* **115**, 011301 (2015).

- [73] T. Okumura *et al.*, The Subaru FMOS galaxy redshift survey (FastSound). IV. New constraint on gravity theory from redshift space distortions at  $z \sim 1.4$ , *Publ. Astron. Soc. Jpn.* **68**, 38 (2016).
- [74] D. Huterer, D. Shafer, D. Scolnic, and F. Schmidt, Testing  $\Lambda$ CDM at the lowest redshifts with SN Ia and galaxy velocities, *J. Cosmol. Astropart. Phys.* **05** (2017) 015.
- [75] A. Pezzotta *et al.*, The VIMOS public extragalactic redshift survey (VIPERS): The growth of structures at  $0.5 < z < 1.2$  from redshift-space distortions in the clustering of the PDR-2 final sample, [arXiv:1612.05645](https://arxiv.org/abs/1612.05645).
- [76] S. Alam *et al.* (BOSS Collaboration), The clustering of galaxies in the completed SDSS-III Baryon Oscillation Spectroscopic Survey: cosmological analysis of the DR12 galaxy sample, [arXiv:1607.03155](https://arxiv.org/abs/1607.03155).
- [77] M. J. Wilson, Ph.D. thesis, Edinburgh University, 2016.
- [78] A. De Felice, S. Mukohyama, and S. Tsujikawa, Density perturbations in general modified gravitational theories, *Phys. Rev. D* **82**, 023524 (2010).
- [79] S. Tsujikawa, Matter density perturbations and effective gravitational constant in modified gravity models of dark energy, *Phys. Rev. D* **76**, 023514 (2007).
- [80] A. De Felice and S. Tsujikawa,  $f(R)$  theories, *Living Rev. Relativ.* **13**, 3 (2010).
- [81] S. Nesseris and A. Mazumdar, Newton's constant in  $f(R, R_{\mu\nu}R^{\mu\nu}, \square R)$  theories of gravity and constraints from BBN, *Phys. Rev. D* **79**, 104006 (2009).
- [82] J. C. Bueno Sanchez and L. Perivolaropoulos, Evolution of dark energy perturbations in scalar-tensor cosmologies, *Phys. Rev. D* **81**, 103505 (2010).
- [83] V. Silveira and I. Waga, Decaying Lambda cosmologies and power spectrum, *Phys. Rev. D* **50**, 4890 (1994).
- [84] W. J. Percival, Cosmological structure formation in a homogeneous dark energy background, *Astron. Astrophys.* **443**, 819 (2005).
- [85] M. Abramowitz, *Handbook of Mathematical Functions, With Formulas, Graphs, and Mathematical Tables* (Dover, New York, 1974).
- [86] W. J. Percival and M. White, Testing cosmological structure formation using redshift-space distortions, *Mon. Not. R. Astron. Soc.* **393**, 297 (2009).
- [87] S. Nesseris and L. Perivolaropoulos, Crossing the phantom divide: Theoretical implications and observational status, *J. Cosmol. Astropart. Phys.* **01** (2007) 018.
- [88] S. Alam, S. Ho, and A. Silvestri, Testing deviations from  $\Lambda$ CDM with growth rate measurements from six large-scale structure surveys at  $z = 0.06-1$ , *Mon. Not. R. Astron. Soc.* **456**, 3743 (2016).
- [89] E. Macaulay, I. Kathrine Wehus, and H. Kristian Eriksen, Lower Growth Rate from Recent Redshift Space Distortion Measurements than Expected from Planck, *Phys. Rev. Lett.* **111**, 161301 (2013).
- [90] S. Basilakos and S. Nesseris, Testing Einstein's gravity and dark energy with growth of matter perturbations: Indications for new physics?, *Phys. Rev. D* **94**, 123525 (2016).
- [91] A. de la Cruz-Dombriz, A. Dobado, and A. Lopez Maroto, On the evolution of density perturbations in  $f(R)$  theories of gravity, *Phys. Rev. D* **77**, 123515 (2008).
- [92] W. Hu and I. Sawicki, Models of  $f(R)$  cosmic acceleration that evade solar-system tests, *Phys. Rev. D* **76**, 064004 (2007).
- [93] S. Basilakos, S. Nesseris, and L. Perivolaropoulos, Observational constraints on viable  $f(R)$  parametrizations with geometrical and dynamical probes, *Phys. Rev. D* **87**, 123529 (2013).
- [94] E.-M. Mueller, W. Percival, E. Linder, S. Alam, G.-B. Zhao, A. G. Sanchez, and F. Beutler, The clustering of galaxies in the completed SDSS-III Baryon Oscillation Spectroscopic Survey: constraining modified gravity, [arXiv:1612.00812](https://arxiv.org/abs/1612.00812).
- [95] E. V. Linder, Cosmic growth history and expansion history, *Phys. Rev. D* **72**, 043529 (2005).
- [96] C. Di Porto and L. Amendola, Observational constraints on the linear fluctuation growth rate, *Phys. Rev. D* **77**, 083508 (2008).
- [97] S. Nesseris and L. Perivolaropoulos, Testing Lambda CDM with the growth function  $\delta(a)$ : Current constraints, *Phys. Rev. D* **77**, 023504 (2008).
- [98] D. Polarski and R. Gannouji, On the growth of linear perturbations, *Phys. Lett. B* **660**, 439 (2008).
- [99] R. Gannouji and D. Polarski, The growth of matter perturbations in some scalar-tensor DE models, *J. Cosmol. Astropart. Phys.* **05** (2008) 018.
- [100] R. Gannouji, B. Moraes, and D. Polarski, The growth of matter perturbations in  $f(R)$  models, *J. Cosmol. Astropart. Phys.* **02** (2009) 034.
- [101] Y. Gong, The growth factor parameterization and modified gravity, *Phys. Rev. D* **78**, 123010 (2008).
- [102] J. Kwan, G. F. Lewis, and E. V. Linder, Mapping growth and gravity with robust redshift space distortions, *Astrophys. J.* **748**, 78 (2012).
- [103] G. Pantazis, S. Nesseris, and L. Perivolaropoulos, Comparison of thawing and freezing dark energy parametrizations, *Phys. Rev. D* **93**, 103503 (2016).
- [104] P. D. Scharre and C. M. Will, Testing scalar tensor gravity using space gravitational wave interferometers, *Phys. Rev. D* **65**, 042002 (2002).
- [105] E. Poisson and C. M. Will, Gravitational waves from inspiraling compact binaries: Parameter estimation using second postNewtonian wave forms, *Phys. Rev. D* **52**, 848 (1995).
- [106] M. Chevallier and D. Polarski, Accelerating universes with scaling dark matter, *Int. J. Mod. Phys. D* **10**, 213 (2001).
- [107] V. Sahni, A. Shafieloo, and A. A. Starobinsky, Model independent evidence for dark energy evolution from Baryon Acoustic Oscillations, *Astrophys. J.* **793**, L40 (2014).
- [108] Encyclopedia of Mathematics, Chaplygin theorem, [http://www.encyclopediaofmath.org/index.php?title=Chaplygin\\_theorem&oldid=18838](http://www.encyclopediaofmath.org/index.php?title=Chaplygin_theorem&oldid=18838), 2011 [accessed March 12, 2017].
- [109] A. Hojjati, L. Pogosian, and G.-B. Zhao, Testing gravity with CAMB and CosmoMC, *J. Cosmol. Astropart. Phys.* **08** (2011) 005.
- [110] N. Aghanim *et al.* (Planck Collaboration), Planck 2015 results. XI. CMB power spectra, likelihoods, and robustness of parameters, *Astron. Astrophys.* **594**, A11 (2016).

- [111] L. Amendola, Non-Gaussian likelihood function, [arXiv: astro-ph/9504029](#).
- [112] P. A. R. Ade *et al.* (Planck Collaboration), Planck 2015 results. XV. Gravitational lensing, *Astron. Astrophys.* **594**, A15 (2016).
- [113] D. Alonso, E. Bellini, P. G. Ferreira, and M. Zumalacarre-gui, Observational future of cosmological scalar-tensor theories, *Phys. Rev. D* **95**, 063502 (2017).
- [114] L. Perenon, F. Piazza, C. Marinoni, and L. Hui, Phenomenology of dark energy: General features of large-scale perturbations, *J. Cosmol. Astropart. Phys.* **11** (2015) 029.
- [115] L. Perenon, C. Marinoni, and F. Piazza, Diagnostic of Horndeski theories, *J. Cosmol. Astropart. Phys.* **01** (2017) 035.
- [116] M. Berg, I. Buchberger, J. Enander, E. Mortsell, and S. Sjors, Growth histories in bimetric massive gravity, *J. Cosmol. Astropart. Phys.* **12** (2012) 021.
- [117] See Supplemental Material at <http://link.aps.org/supplemental/10.1103/PhysRevD.96.023542> for the *Mathematica* files used for the production of the figures as well as the figures themselves.